

Scope and convergence of the hopping parameter expansion in finite temperature QCD with heavy quarks around the critical point

Naoki Wakabayashi¹, Shinji Ejiri², Kazuyuki Kanaya³, and Masakiyo Kitazawa^{4,5}

¹*Graduate School of Science and Technology, Niigata University, Niigata 950-2181, Japan*

²*Department of Physics, Niigata University, Niigata 950-2181, Japan*

³*Tomonaga Center for the History of the Universe, University of Tsukuba, Tsukuba, Ibaraki 305-8571, Japan*

⁴*Department of Physics, Osaka University, Toyonaka, Osaka 560-0043, Japan*

⁵*J-PARC Branch, KEK Theory Center, Institute of Particle and Nuclear Studies, KEK, 203-1, Shirakata, Tokai, Ibaraki, 319-1106, Japan*

.....
Hopping parameter expansion is a useful tool to investigate heavy dynamical quarks in lattice QCD, while the range of its applicability has been sometimes questioned. We study the convergence and the valid range of the hopping parameter expansion in the determination of the critical point (critical quark mass) of QCD with heavy quarks at finite temperature and density. On lattices with sufficiently large spatial extent, the terms in the hopping parameter expansion are classified into Wilson loop terms and Polyakov-type loop terms. We first study the case of the worst convergence in which all the gauge link variables are unit matrices and thus the Wilson loops and the Polyakov-type loops get their maximum values. We perform explicit calculation up to more than 100th order of the hopping parameter expansion. We show that the hopping parameter expansion is convergent up to the chiral limit of free Wilson quarks. We then perform a Monte-Carlo simulation to measure correlation among Polyakov-type loop terms up to the 20th order of the hopping parameter expansion. In previous studies, strong correlation between the leading order Polyakov loop term and the next-to-leading order bent Polyakov loop terms was reported and used to construct an effective theory to incorporate the next-to-leading order effect by a shift of the leading order coupling parameter. We establish that the strong correlation among Polyakov-type loop terms holds also at higher orders of the hopping parameter expansion, and extend the effective theory to incorporate higher-order effects up to high orders. Using the effective theory, we study the truncation error of the hopping parameter expansion. We find that the previous next-to-leading order result of the critical point for $N_t = 4$ are well reliable. For $N_t \geq 6$, we need to incorporate higher-order effects in the effective theory.

1 Introduction

Quantum chromodynamics (QCD) is the fundamental theory of quarks and gluons. When all quarks are infinitely heavy, QCD tends to be pure gauge SU(3) Yang-Mills theory (quenched QCD), which is confining at low temperatures but turns into a deconfining phase by a first order deconfinement phase transition. This transition becomes weaker as the quark mass decreases, and eventually changes to a crossover at a critical point (critical quark mass). Identification of the critical point is important in understanding the phase structure of QCD.

In the determination of the critical point in lattice QCD with heavy quarks, the hopping parameter expansion has played important roles: It enables us to carry out several analytic studies and also helps us in reducing much the computational demands. On the other hand, the range of its applicability has been questioned sometimes. In particular, we need to estimate the systematic error caused by the truncation of higher-order terms in the hopping parameter expansion.

To determine the phase transition point and to investigate the properties of the phase transition, we need to calculate the order parameter as a continuous function of temperature and quark mass. The reweighting method is useful for calculating physical quantities as continuous functions by Monte Carlo simulations [1]. However, in order to apply the reweighting method to investigate the quark mass dependence, it is necessary to calculate the quark determinant, which requires large computational costs. Therefore, in Refs. [2–4], the reweighting method was performed by Taylor-expanding the quark determinant with the hopping parameters and calculating the expansion coefficients. To investigate the heavy quark region, the Taylor expansion around zero hopping parameter (hopping parameter expansion) is useful. The reweighting factor can be given by calculating Wilson loops and Polyakov loops, and the reweighting factor adds the effect of dynamic quarks to the quenched QCD simulations.

In Refs. [5–8], the method by the hopping parameter expansion was adopted to investigate the critical point of QCD with heavy quarks on $N_t = 4$ and 6 lattices, where N_t is the temporal extent of the lattice. This method was extended to finite densities in Refs. [6, 9]. In Refs. [6, 7], an effective method was proposed to incorporate the next-to-leading order effect of bent Polyakov loops by a shift of the coefficient for the leading-order Polyakov loop term, and the truncation error was estimated from the difference between the leading-order and the next-to-leading order calculations. In Ref. [8], a finite size scaling analysis was adopted to obtain the critical point in the thermodynamic limit, where, to overcome the overlapping problem on spatially large lattices, the configurations are generated by an action incorporating the leading-order effect by the Polyakov loop term, and the next-to-leading order effect is taken into account by the reweighting. The hopping parameter expansion was applied also to QCD with mixed heavy and light quarks [9, 10].

From these studies, it was found that the hopping parameter for the critical point κ_c increases as N_t increases. Similar trend is observed also in recent full QCD studies [11, 12]. At the critical point of $N_t = 4$, the effect of next-to-leading order was found to be small, while at that of $N_t = 6$, the effect of next-to-leading order turned out to be significant. As N_t increases further, the truncation error of higher-order terms will increase in the determination of the critical point. This means that, when N_t exceeds a certain value, the critical point would move into a region where the hopping parameter expansion is not applicable. Therefore, it is important to confirm the reliability of the resulting κ_c .

In this paper, we study the convergence and the valid range of the hopping parameter expansion in the determination of the critical point in QCD with heavy quarks. In Sec. 2, we introduce our model and the hopping parameter expansion, and discuss our method to calculate the expansion terms. To obtain the lower bound of the convergence radius of the hopping parameter expansion, in Sec. 3, we first consider the case of the worst convergence by setting all link variables to unit matrices, and study the convergence radius by explicitly calculating the expansion terms up to high orders in this case. In Sec. 4, we then study the effect of high order expansion terms and the systematic error due to truncation of the expansion series, and confirm if the previous calculation of the critical point for $N_t = 4$ and 6 lattices by the hopping parameter expansion is within the valid range. We also discuss that calculation of κ_c for $N_t = 8$ will be also possible when we combine the calculation with an effective theory which incorporates higher-order effects of the hopping parameter expansion. The effective theory is an extension of the effective theory developed in Refs. [6, 7] to high orders, and is based on the strong correlation among Polyakov-type loops. By performing Monte Carlo simulations in Sec. 5, we explicitly show that the Polyakov-type loops are strongly correlated up to high orders, and calculate the coefficients for the effective theory. Using the coefficients thus obtained, we then calculate the critical point in $2 + 1$ -flavor QCD incorporating the higher-order effect. Section 6 is devoted to a discussion for the case of non-zero densities. Finally, we summarize and conclude in Sec. 7.

2 Hopping parameter expansion

We study lattice QCD with N_f flavors of quarks on an $N_s^3 \times N_t$ lattice. For gluons, we adopt the standard plaquette gauge action given by

$$S_g = -6N_{\text{site}} \beta \hat{P}, \quad (1)$$

with $\beta = 2N_c/g^2$ the gauge coupling parameter, $N_{\text{site}} = N_s^3 N_t$ the space-time lattice volume, $N_c = 3$ the number of colors, and \hat{P} the plaquette operator defined by

$$\hat{P} = \frac{1}{6N_{\text{site}}N_c} \sum_{x, \mu < \nu} \text{Re tr}_c \left[U_{x,\mu} U_{x+\hat{\mu},\nu} U_{x+\hat{\nu},\mu}^\dagger U_{x,\nu}^\dagger \right], \quad (2)$$

where $U_{x,\mu}$ is the gauge link variable in the μ direction at site x , $x + \hat{\mu}$ is the next site in the μ direction from x , and tr_c means the trace over the color index. For quarks, we adopt the standard Wilson quark action given by

$$S_q = \sum_{f=1}^{N_f} \sum_{x,y} \bar{\psi}_x^{(f)} M_{xy}(\kappa_f) \psi_y^{(f)}, \quad (3)$$

where M_{xy} is the Wilson quark kernel

$$\begin{aligned} M_{xy}(\kappa_f) &= \delta_{xy} - \kappa_f \sum_{\mu=1}^4 \left[(1 - \gamma_\mu) U_{x,\mu} \delta_{y,x+\hat{\mu}} + (1 + \gamma_\mu) U_{y,\mu}^\dagger \delta_{y,x-\hat{\mu}} \right] \\ &\equiv \delta_{xy} - \kappa_f B_{xy} \end{aligned} \quad (4)$$

and κ_f is the hopping parameter for the f -th flavor which is related to the bare quark mass m_f by $\kappa_f = 1/(2am_f + 8)$ with a the lattice spacing.

For simplicity, we mainly consider the case of degenerate N_f flavors in this paper unless otherwise stated. Then the expectation value of an operator \mathcal{O} is given by

$$\langle \mathcal{O} \rangle_{(\beta, \kappa)} = \frac{\int \mathcal{D}U \mathcal{O} [\det M(\kappa)]^{N_f} e^{6\beta N_{\text{site}} \hat{P}}}{\int \mathcal{D}U [\det M(\kappa)]^{N_f} e^{6\beta N_{\text{site}} \hat{P}}}. \quad (5)$$

To study QCD in the vicinity of the heavy quark limit $\kappa = 0$, we perform the hopping parameter expansion of $\det M(\kappa)$ around $\kappa = 0$. For the effective quark action $\ln \det M(\kappa)$ we find

$$\ln \det M(\kappa) = \ln \det M(0) + N_{\text{site}} \sum_{n=1}^{\infty} D_n \kappa^n, \quad (6)$$

where

$$D_n = \frac{1}{N_{\text{site}} n!} \left[\frac{\partial^n \ln \det M(\kappa)}{\partial \kappa^n} \right]_{\kappa=0} = \frac{(-1)^{n+1} (n-1)!}{N_{\text{site}} n!} \text{Tr} \left[\left(M^{-1} \frac{\partial M}{\partial \kappa} \right)^n \right]_{\kappa=0}. \quad (7)$$

Since $M(0) = 1$ for the Wilson fermion, the first term $\ln \det M(0)$ vanishes in Eq. (6), and M^{-1} in Eq. (7) can be neglected. We thus find

$$D_n = \frac{-1}{N_{\text{site}} n} \text{Tr} [B^n], \quad (8)$$

with $B_{xy} = -(\partial M / \partial \kappa)_{xy}$ the hopping term defined in Eq. (4).

Non-vanishing contributions to the trace of Eq. (8) appear only when the product of the hopping terms forms a closed loop in the space-time. We classify the closed loops in D_n by the winding number m which counts the number of windings in the temporal direction without distinguishing the positive and negative directions, and decompose D_n as

$$D_n = W(n) + \sum_{m=1}^{\infty} L_m(N_t, n) \equiv W(n) + L(N_t, n), \quad (9)$$

where the first term $W(n)$ for $m = 0$ is the summation of various n -step Wilson loops, and $L_m(N_t, n)$ is the summation of n -step Polyakov-type loops with the winding number m . Here, $L_m(N_t, n)$ can be further decomposed as $L_m = L_m^+ + L_m^-$ with L_m^+ going in the positive direction and L_m^- going in the negative direction. These are complex numbers with $L_m^- = (L_m^+)^*$, and have the properties of $L_m = L_m^+ + L_m^- = 2\text{Re} L_m^+$ and $L_m^+ - L_m^- = 2i \text{Im} L_m^+$.

In Eq. (9), the range of m is actually finite for each n : $L_m(N_t, n)$ vanishes when $n < mN_t$. For simplicity, we assume that N_t is even in the followings, though extension to odd N_t 's is straightforward. When N_t is even, $L_m(N_t, n) = 0$ also at odd n 's, and thus we have non-zero D_n only at even n 's.

In the calculation of closed loops, when the loop winds around the lattice, we need to take into account the effect of boundary conditions: When the hopping term B is multiplied by the $4N_c N_{\text{site}}$ -component pseudo-quark field ψ , ψ satisfies the following anti-periodic boundary condition in the temporal direction

$$\psi(x_1, x_2, x_3, x_4 - N_t) = -\psi(x_1, x_2, x_3, x_4). \quad (10)$$

As a result of Eq. (10), one must apply a factor of $(-1)^m$ in the calculation of Polyakov-type loops with the winding number m . For the influence of spatial boundary conditions, we assume that N_s is sufficiently large such that we do not need to consider that through spatial windings.

We define each of the Wilson and Polyakov-type loops as the average over the space-time position and normalize them such that they become unity when all $U_{x,\mu}$'s are set to the unit matrix. The first several terms of Eq. (9) are then given by

$$W(4) = 96N_c\hat{P}, \quad (11)$$

$$W(6) = 256N_c \left(3\hat{W}_{\text{rec}} + 6\hat{W}_{\text{chair}} + 2\hat{W}_{\text{crown}} \right), \quad (12)$$

$$L_1(N_t, N_t) = \frac{4N_c \times 2^{N_t}}{N_t} \text{Re}\hat{\Omega}, \quad (13)$$

$$L_1(N_t, N_t + 2) = 12N_c \times 2^{N_t} \left(2 \sum_{k=1}^{N_t/2-1} \text{Re}\hat{\Omega}_k + \text{Re}\hat{\Omega}_{N_t/2} \right). \quad (14)$$

Here, \hat{W}_{rec} , \hat{W}_{chair} , and \hat{W}_{crown} are 6-step Wilson loops with rectangular, chair-shaped, and crown-shaped loops, respectively, which are averaged over the space-time position on each configuration. $\hat{\Omega}$ is the Polyakov loop defined as

$$\hat{\Omega} = \frac{1}{N_c N_s^3} \sum_{\vec{x}} \text{tr}_c \left[U_{\vec{x},4} U_{\vec{x}+\hat{4},4} U_{\vec{x}+2\cdot\hat{4},4} \cdots U_{\vec{x}+(N_t-1)\cdot\hat{4},4} \right] \quad (15)$$

with $\sum_{\vec{x}}$ for a summation over the sites on a time slice, and $\hat{\Omega}_k$'s are bent Polyakov loops with $N_t + 2$ steps. See Refs. [7, 8] for the definition of \hat{W}_{rec} etc. and $\hat{\Omega}_k$.

2.1 Calculation of $W(n)$ and $L_m(N_t, n)$

Effects of $W(n)$ and $L_m(N_t, n)$ can be in part separated by adopting different temporal boundary conditions. For the case of periodic boundary condition at the temporal boundary, the n -th coefficient D_n of the hopping parameter expansion of $\ln \det M(\kappa)$ is changed to

$$D_n^+ = W(n) + \sum_{m=1}^{\infty} (-1)^m L_m(N_t, n). \quad (16)$$

Here, $(-1)^m$ is multiplied because $L_m(N_t, n)$ is defined with the anti-periodic boundary condition. Combining D_n and D_n^+ , we can separate the contributions of even and odd winding numbers as

$$\frac{D_n + D_n^+}{2} = W(n) + \sum_{m=1}^{\infty} L_{2m}(N_t, n), \quad (17)$$

$$\frac{D_n - D_n^+}{2} = \sum_{m=1}^{\infty} L_{2m-1}(N_t, n). \quad (18)$$

These relations enables us to determine $W(n)$ and $L_1(N_t, n)$ for small n :

$$W(n) = \frac{D_n + D_n^+}{2} \quad \text{for } n < 2N_t, \quad (19)$$

$$L_1(N_t, n) = \frac{D_n - D_n^+}{2} \quad \text{for } n < 3N_t. \quad (20)$$

We can further decompose the contributions of Wilson and Polyakov-type loop terms by introducing twisted boundary conditions at the temporal boundary. To show the case to decompose m

in modulus 4, we impose a boundary condition $\psi(x_1, x_2, x_3, x_4 - N_t) = i\psi(x_1, x_2, x_3, x_4)$ or equivalently $\psi(x_1, x_2, x_3, x_4 + N_t) = -i\psi(x_1, x_2, x_3, x_4)$. Then the n -th coefficient of $\ln \det M(\kappa)$ with this boundary condition reads

$$\begin{aligned} D_n^i &= W(n) + \sum_{m=1}^{\infty} (-i)^m L_m^+(N_t, n) + \sum_{m=1}^{\infty} i^m L_m^-(N_t, n) \\ &= W(n) + \sum_{m=1}^{\infty} (-1)^m L_{2m}(N_t, n) - 2 \sum_{m=1}^{\infty} (-1)^m \text{Im} L_{2m-1}^+(N_t, n). \end{aligned} \quad (21)$$

Similarly, when we impose the boundary condition $\psi(x_1, x_2, x_3, x_4 - N_t) = -i\psi(x_1, x_2, x_3, x_4)$, we find

$$D_n^{-i} = W(n) + \sum_{m=1}^{\infty} (-1)^m L_{2m}(N_t, n) + 2 \sum_{m=1}^{\infty} (-1)^m \text{Im} L_{2m-1}^+(N_t, n) \quad (22)$$

Combining them, we obtain relations including

$$\frac{D_n + D_n^+ + D_n^i + D_n^{-i}}{4} = W(n) + \sum_{m=1}^{\infty} L_{4m}(N_t, n), \quad (23)$$

$$\frac{D_n + D_n^+ - D_n^i - D_n^{-i}}{4} = \sum_{m=1}^{\infty} L_{4m-2}(N_t, n). \quad (24)$$

From the last equation, we find that $L_2(N_t, n) = (D_n + D_n^+ - D_n^i - D_n^{-i})/4$ when $n < 6N_t$.

The separation of D_n into $W(n)$ and $L_m(N_t, n)$ can be established more generally by combining the values of $\text{Tr}[B^n]$ calculated with various twisted boundary conditions. If we impose the boundary condition:

$$\psi(x_1, x_2, x_3, x_4 - N_t) = e^{i\theta} \psi(x_1, x_2, x_3, x_4), \quad (25)$$

the expansion term, denoted by D_n^θ , becomes

$$\begin{aligned} D_n^\theta &= W(n) + \sum_{m=1}^{\infty} (-1)^m e^{im\theta} L_m^+(N_t, n) + \sum_{m=1}^{\infty} (-1)^m e^{-im\theta} L_m^-(N_t, n) \\ &= W(n) + \sum_{m=1}^{\infty} (-1)^m \cos(m\theta) L_m(N_t, n) + 2 \sum_{m=1}^{\infty} (-1)^m \sin(m\theta) \text{Im} L_m^+(N_t, n). \end{aligned} \quad (26)$$

Then,

$$\frac{D_n^\theta + D_n^{(2\pi-\theta)}}{2} = W(n) + \sum_{m=1}^{\infty} (-1)^m \cos(m\theta) L_m(N_t, n). \quad (27)$$

Let $D_{n,w}$ be the value of $(-1/N_{\text{site}}n)\text{Tr}[B^n]$ calculated with the twisted boundary condition with $\theta = \pi w/Y$, i.e., $\psi(x_1, x_2, x_3, x_4 - N_t) = e^{i\pi w/Y} \psi(x_1, x_2, x_3, x_4)$, where Y is the maximum winding number, i.e., the largest integer satisfying $Y \leq n/N_t$, and $w = 0, 1, \dots, 2Y - 1$. Then $W(n)$ and

$\tilde{L}_m(N_t, n) = (-1)^m L_m(N_t, n)$ are related to $D_{n,w}$ as

$$\begin{bmatrix} D_{n,0} \\ (D_{n,1} + D_{n,2Y-1})/2 \\ \vdots \\ (D_{n,Y-1} + D_{n,Y+1})/2 \\ D_{n,Y} \end{bmatrix} = G \begin{bmatrix} W(n) \\ \tilde{L}_1(N_t, n) \\ \vdots \\ \tilde{L}_{Y-1}(N_t, n) \\ \tilde{L}_Y(N_t, n) \end{bmatrix}, \quad (28)$$

where G is a $(Y+1) \times (Y+1)$ matrix whose components are given by $G_{jk} = \cos(\pi jk/Y)$ with $j, k = 0, 1, \dots, Y$. By inversely solving Eq. (28) one obtains $W(n)$ and $L_m(N_t, n)$ for $m = 1, \dots, Y$. In particular, $W(n)$ is given by

$$W(n) = \frac{1}{2Y} \sum_{w=0}^{2Y-1} D_{n,w}. \quad (29)$$

3 Expansion coefficients and convergence radius for the case $U_{x,\mu} = \mathbf{1}$

In this section, we calculate the Wilson loop terms $W(n)$ and the Polyakov-type loop terms $L_m(N_t, n)$ in the weak coupling limit, i.e., in the case that all link variables are set to the unit matrix, $U_{x,\mu} = \mathbf{1}$. We denote $W(n)$ and $L_m(N_t, n)$ for the case $U_{x,\mu} = \mathbf{1}$ as $W^0(n)$ and $L_m^0(N_t, n)$, respectively. In this case, the Wilson loops and Polyakov loops in $W(n)$ and $L_m(N_t, n)$ get their maximum value one. Because the variety of n -step loops increase rapidly with n , the absolute values of $W^0(n)$ and $L_m^0(N_t, n)$ increase rapidly as n increases. On the other hand, because the values of the loops on actual configurations at $\beta < \infty$ decrease exponentially as n increases, the ratios $|W/W^0|$ and $|L_m/L_m^0|$ are at most one and are decreasing functions of n . Thus, information of $W^0(n)$ and $L_m^0(N_t, n)$ gives lower bounds for the convergence radius of the hopping parameter expansion. In Sec. 5, we study the ratios $|W/W^0|$ and $|L_m/L_m^0|$ on actual configurations by a Monte-Carlo simulation.

3.1 Numerical values for $W^0(n)$ and $L_m^0(N_t, n)$

Setting $N_c = 3$, the first several terms are obtained from Eqs. (11)–(14) as

$$\begin{aligned} W^0(4) &= 288, \quad W^0(6) = 768 \times (3 + 6 + 2) = 8448, \\ L_1^0(N_t, N_t) &= \frac{12 \times 2^{N_t}}{N_t}, \quad L_1^0(N_t, N_t + 2) = 36 \times 2^{N_t}(N_t - 1). \end{aligned} \quad (30)$$

For the present case of $U_{x,\mu} = \mathbf{1}$, we can also show

$$L_m^0(N_t, n) = (-1)^{m-1} L_1^0(mN_t, n). \quad (32)$$

Using this property, we can calculate some L_m^0 for $m > 1$ by substituting L_1^0 of Eq. (31).

We calculate D_n for $U_{x,\mu} = \mathbf{1}$ on a lattice with an N_t and sufficiently large N_s . Since the link variables are uniform in this case, calculation of one diagonal element for the position index is sufficient. For the color and spinor indexes, we take the trace over them. More concretely, we prepare a pseudo-fermion field \vec{e}_i having non-vanishing element only at a position and at the i -th combination of the color and spinor indexes, we calculate the diagonal element $[B^n]_{ii} = \vec{e}_i^\dagger B^n \vec{e}_i$ for all combinations of i . We then calculate D_n from $\sum_{i=1}^{4N_c} [B^n]_{ii}$.

Table 1 Wilson loop terms $W^0(n)$ for the case $U_{x,\mu} = 1$.

$W^0(4)$	288	$W^0(20)$	$1.54422361 \times 10^{14}$	$W^0(36)$	$-5.58410362 \times 10^{27}$
$W^0(6)$	8 448	$W^0(22)$	$2.83682900 \times 10^{15}$	$W^0(38)$	$-2.91018925 \times 10^{29}$
$W^0(8)$	245 952	$W^0(24)$	$-2.40028584 \times 10^{16}$	$W^0(40)$	$-1.50223497 \times 10^{31}$
$W^0(10)$	7 372 800	$W^0(26)$	$-6.88836562 \times 10^{18}$	$W^0(42)$	$-7.71380102 \times 10^{32}$
$W^0(12)$	225 232 896	$W^0(28)$	$-5.41133954 \times 10^{20}$	$W^0(44)$	$-3.95168998 \times 10^{34}$
$W^0(14)$	6 906 175 488	$W^0(30)$	$-3.39122203 \times 10^{22}$	$W^0(46)$	$-2.02386871 \times 10^{36}$
$W^0(16)$	208 431 502 848	$W^0(32)$	$-1.93668514 \times 10^{24}$	$W^0(48)$	$-1.03783044 \times 10^{38}$
$W^0(18)$	$6.00259179 \times 10^{12}$	$W^0(34)$	$-1.05424635 \times 10^{26}$	$W^0(50)$	$-5.33468075 \times 10^{39}$

To compute D_n up to $n = n_{max}$ on lattices with $N_t = 4, 6, \dots, n_{max}/2 + 1$, the spatial lattice size $N_s = n_{max} + 2$ is sufficient. We also compute D_n^+ with the periodic boundary condition. For $n < 2N_t$ and $n < N_s$, $W^0(n)$ is given by Eq. (19). We compute D_n and D_n^+ on a $56^3 \times 28$ lattice. The results of $W^0(n)$ are listed in Table 1 up to $n = 50$. The sum of the Polyakov-type loop terms,

$$L^0(N_t, n) = \sum_{m=1}^{\infty} L_m^0(N_t, n), \quad (33)$$

is then obtained by $L^0(N_t, n) = D_n(N_t) - W^0(n)$. The terms corresponding to each loop in $W(n)$ and $L_m(N_t, n)$ can take both positive and negative signs depending on the product of gamma matrices of the hopping term Eq. (4), and, in the case of Polyakov-type loops, also on the temporal boundary condition. The total sign of $W(n)$ and $L_m(N_t, n)$ is determined by which sign is dominant.

For each of the Polyakov-type loop terms $L_m^0(N_t, n)$, we measure D_n and D_n^+ up to $n = 30$ for the case $U_{x,\mu} = 1$ on lattices with $N_s = 32$ and $N_t = 4-24$. We first calculate $L_1^0(N_t, n)$ for $n < 3N_t$ by Eq. (20) for each N_t , and then $L_m^0(N_t, n)$ for $m \geq 2$ as much as possible by Eq. (32). When $n < 5N_t$, we also have the equation $L_1^0(N_t, n) = (D_n - D_n^+)/2 - L_1(2N_t, n)$, and when $n < 7N_t$, $L_1^0(N_t, n) = (D_n - D_n^+)/2 - L_1^0(2N_t, n) - L_1^0(3N_t, n)$. By repeating this procedure, $L_m^0(N_t, n)$ is calculated for all values of m . The results for $n \leq 30$ are summarized in Table 2. In this table, the theoretical value of Eq. (31) is given when available. We find that, for these values of (N_t, n) , the term with $m = 1$ is dominant and the contributions of the terms with $m = 2-4$ are small.

3.2 Alternative method to calculate $W^0(n)$ and $L_m^0(N_t, n)$

In Sec. 2.1, we have shown that the values of $L_m(N_t, n)$ for individual winding numbers m can be calculated by combining D_n^θ obtained with various twisted boundary conditions Eq. (25). For the case $U_{x,\mu} = 1$, because of the uniformity of the system one finds by extending this idea that $W^0(n)$ and $L_m^0(N_t, n)$ are calculable on the lattice with temporal extent of any divisor of N_t . Pursuing this idea leads to the conclusion that the calculation can be carried out on the $N_s^3 \times 1$ lattice by combining D_n^θ with $\theta = \pi w/N_t Y$ with $w = 0, 1, 2, \dots, 2N_t Y$.

There is no reason not to apply the same idea to all spatial directions. Then, after folding all the spatial directions one finally finds that the calculation is feasible just on 1^4 lattice. Since the spatial coordinates no longer exist in this limit, in this case the “hopping” term is given by the

following 4×4 matrix:

$$b(\varphi) = b(\varphi_1, \varphi_2, \varphi_3, \varphi_4) = \sum_{\mu=1}^4 \left[(1 - \gamma_\mu) e^{i\varphi_\mu} + (1 + \gamma_\mu) e^{-i\varphi_\mu} \right], \quad (34)$$

where φ_μ is the phase of the “twisted boundary conditions” for the μ -th direction. Using Eq. (34), the value of D_n on the N_s^4 lattice with the periodic boundary conditions for all directions is calculated to be

$$D_{n;N_s^4} = -\frac{N_c}{n} \frac{1}{N_s^4} \sum_{k_1, k_2, k_3, k_4=1}^{N_s} \text{tr}_D \left[b \left(\frac{2\pi k_1}{N_s}, \frac{2\pi k_2}{N_s}, \frac{2\pi k_3}{N_s}, \frac{2\pi k_4}{N_s} \right)^n \right], \quad (35)$$

where tr_D is the trace over the Dirac index. This result leads to

$$W^0(n) = D_{n;N_s^4} \quad (n < N_s). \quad (36)$$

Next, the value of D_n^θ on the $N_s^3 \times N_t$ lattice is similarly obtained as

$$D_{n;N_s^3 \times N_t}^\theta = -\frac{N_c}{n} \frac{1}{N_s^4} \sum_{k_1, k_2, k_3=1}^{N_s} \sum_{k_4=1}^{N_t} \text{tr}_D \left[b \left(\frac{2\pi k_1}{N_s}, \frac{2\pi k_2}{N_s}, \frac{2\pi k_3}{N_s}, \frac{2\pi k_4 + \theta}{N_t} \right)^n \right]. \quad (37)$$

From Eq. (37) one can construct $L_m(N_t, n)$ with a similar manipulation as Eq. (28). Since $L_m^0(N_t, n)$ is always real, one has $D_n^\theta = D_n^{-\theta}$ and thereby only $Y + 1$ calculations of D_n^θ are enough in this analysis. In the large N_s limit, the sum over k_μ in Eqs. (35) and (37) is replaced with an integral: For example, Eq. (35) in this limit reads

$$D_{n;N_s^4} \xrightarrow{N_s \rightarrow \infty} -\frac{N_c}{n} \int_0^{2\pi} \frac{d^4 \varphi}{(2\pi)^4} \text{tr}_D [b(\varphi)^n]. \quad (38)$$

The same result is obtained by directly expanding $\ln \det M(\kappa)$. By Fourier transforming Eq. (4), one has

$$\ln \det M(\kappa) = N_c \int_{-\pi}^{\pi} \frac{d^4 k}{(2\pi)^4} \text{tr}_D \ln \tilde{M}_k(\kappa) \quad (39)$$

with the 4×4 matrix in the Dirac-spinor space

$$\tilde{M}_k(\kappa) = 1 - \kappa b(k) = 1 - 2\kappa \left(\sum_{\mu} \cos k_\mu - i \sum_{\mu} \gamma_\mu \sin k_\mu \right), \quad (40)$$

for $U_{x,\mu} = 1$. Then, one easily finds that the Taylor expansion of Eq. (39) with respect to κ at $\kappa = 0$ gives Eq. (38).

The calculation of $\text{tr}_D[(b(\varphi))^n]$ in Eqs. (35), (37) and (38) is simplified using the fact that the two degenerate eigenvalues of the 4×4 matrix b are given by

$$\lambda_{\pm}(\varphi) = 2 \sum_{\mu} \cos \varphi_\mu \pm 2i \sqrt{\sum_{\mu} \sin^2 \varphi_\mu}. \quad (41)$$

Using Eq. (41) one finds

$$\text{tr}_D [b(\varphi)^n] = 2 \left[(\lambda_+(\varphi))^n + (\lambda_-(\varphi))^n \right]. \quad (42)$$

The eigenvalues Eq. (41) have the maximum absolute value $|\lambda_{\pm}| = 8$ at $\varphi_1 = \varphi_2 = \varphi_3 = \varphi_4 = 0$. Therefore, Eq. (38) grows as 8^n for $n \rightarrow \infty$. This shows that the radius of convergence of the hopping parameter expansion for $U_{x,\mu} = 1$ is $1/8$, i.e., up to the chiral limit of free Wilson fermions.

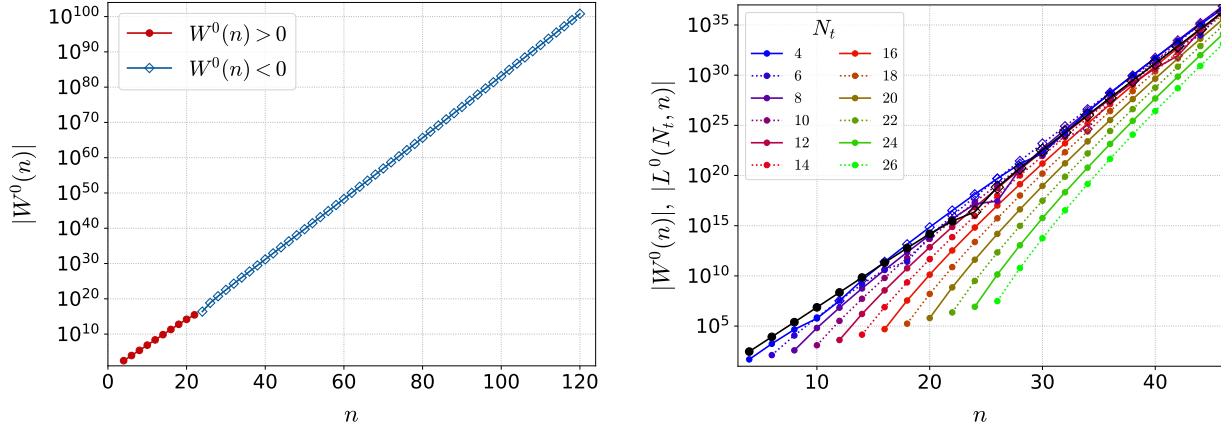


Fig. 1 Absolute values of the Wilson loop term $W^0(n)$ (left) and the sum of Polyakov-type loop terms $L^0(N_t, n)$ (right), computed with setting all $U_{x,\mu} = 1$. In the right panel, results of $|W^0(n)|$ is also shown by black symbols. The closed circle and open diamond symbols mean positive and negative values, respectively.

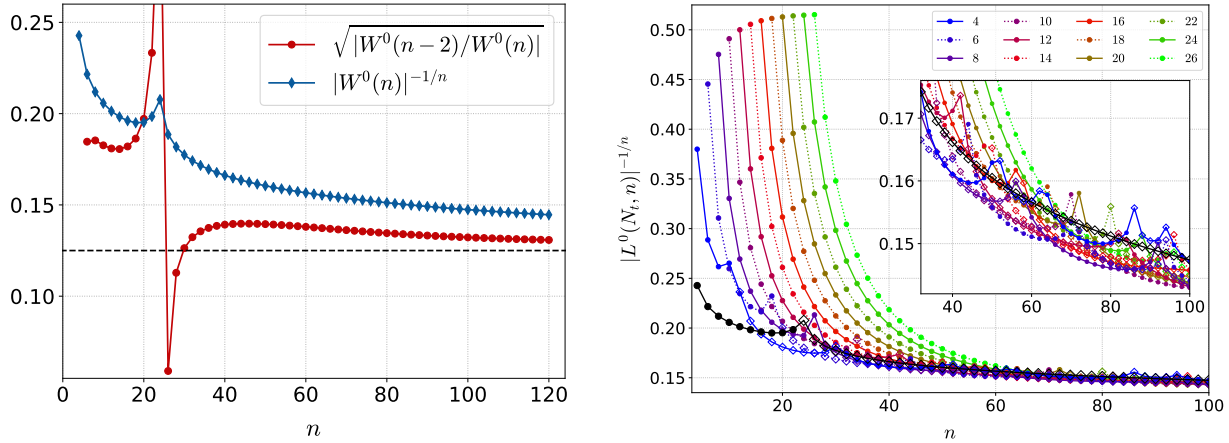


Fig. 2 Test of convergence in the case $U_{x,\mu} = 1$. **Left:** $\kappa_{\text{dA}}(W^0; n) = \sqrt{|W^0(n-2)/W^0(n)|}$ (red symbols) based on the d'Alembert's test and $\kappa_{\text{CH}}(W^0; n) = |W^0(n)|^{-1/n}$ (blue symbols) based on the Cauchy-Hadamard's test, for Wilson loop terms. The horizontal dashed line in black represents the chiral limit $\kappa = 1/8$ for free Wilson fermions. **Right:** $\kappa_{\text{CH}}(L^0; n) = |L^0(N_t, n)|^{-1/n}$ for Polyakov-type loop terms (colored symbols), together with $\kappa_{\text{CH}}(W^0; n)$ (black symbols). The inset in the right panel is a close-up of the range $n = 32-100$.

The above procedure to calculate $W^0(n)$ and $L_m^0(N_t, n)$ enables us to increase n and N_t up to extremely large values without worrying about the memory limitations. We have numerically checked that $W^0(n)$ and $L_m^0(N_t, n)$ obtained from Eqs. (35) and (37) give exactly the same results with those given in Tables 1 and 2.

3.3 Convergence radius

We show the results of $|W^0(n)|$ in the left panel of Fig. 1. The vertical axis is logarithmic. $W^0(n)$ changes its sign at $n = 24$. The closed circle symbol means a positive $W^0(n)$, and the open diamond symbol a negative $W^0(n)$. The results of the absolute value of $|L^0(N_t, n)|$ are given in the right panel of Fig. 1. The sign changes for $N_t = 4$ at $n = 12, 32$ and 52 ; for $N_t = 6$ at $n = 20$ and 44 ; for $N_t = 8$ at $n = 28$; for $N_t = 10$ at $n = 34$; for $N_t = 12$ at $n = 42$; and for $N_t = 14$ at $n = 50$. The open diamond symbol means a negative value, again. As seen in the left and right panels of Fig. 1, $W^0(n)$ and $L^0(N_t, n)$ start from the values of Eqs. (30) and (31) at $n = 4$ and N_t , respectively, and their absolute values increase exponentially with n .

Since $W^0(n)$ and $L^0(N_t, n)$ increase rapidly with n , the hopping parameter expansion does not converge unless $|W^0(n-2)\kappa^{n-2}| > |W^0(n)\kappa^n|$ and $|L^0(N_t, n-2)\kappa^{n-2}| > |L^0(N_t, n)\kappa^n|$ for large n . This leads to d'Alembert's ratio test of convergence,

$$\kappa < \kappa_{\text{dA}}(W^0; n) = \sqrt{\left| \frac{W^0(n-2)}{W^0(n)} \right|}, \quad \kappa < \kappa_{\text{dA}}(L^0; n) = \sqrt{\left| \frac{L^0(N_t, n-2)}{L^0(N_t, n)} \right|} \quad \text{for large } n. \quad (43)$$

Another conventional test of convergence is based on the Cauchy-Hadamard's convergence radius given by

$$\kappa < \kappa_{\text{CH}}(W^0; n) = |W^0(n)|^{-1/n}, \quad \kappa < \kappa_{\text{CH}}(L^0; n) = |L^0(N_t, n)|^{-1/n} \quad \text{for large } n. \quad (44)$$

Because the values of the Wilson loops and the Polyakov-type loops on actual configurations decrease exponentially as n increases, the convergence radius in reality should be larger than the right hand sides of Eqs. (43) and (44), i.e., $\kappa_{\text{dA}}(X; n)$ and $\kappa_{\text{CH}}(X; n)$ at large n provide us with lower bounds for the convergence radius.

In the left panel of Fig. 2, we show $\kappa_{\text{dA}}(W^0; n)$ (red symbols) and $\kappa_{\text{CH}}(W^0; n)$ (blue symbols) as functions of n . The oscillating behavior of the red symbols and the peak of the blue symbols at $n = 24$ is due to the sign change of $W(n)$ there, as shown in the left panel of Fig. 1. This figure shows that, in the large n limit, $\kappa_{\text{dA}}(W^0; n)$ and $\kappa_{\text{CH}}(W^0; n)$ approach $\kappa = 1/8$ shown by the dashed line in the figure. This is in accordance with the discussion in Sec. 3.2.

In the right panel of Fig. 2, we show $\kappa_{\text{CH}}(L^0; n)$ for Polyakov-type loop terms. Since $L^0(N_t, n)$ changes its sign frequently, we plot the results of $\kappa_{\text{CH}}(L^0; n)$ only, because their n -dependence is milder than $\kappa_{\text{dA}}(L^0; n)$. This figure is also consistent with the expectation that $\kappa_{\text{CH}}(L^0; n)$ approaches $1/8$ in the large n limit.

Table 2 Polyakov-type loop expansion terms $L_m^0(N_t, n)$ for the case $U_{x,\mu} = 1$.

$L_1^0(4, 4)$	48	$L_1^0(10, 10)$	1 228.8	$L_1^0(18, 18)$	174 762.67
$L_1^0(4, 6)$	1 728	$L_1^0(10, 12)$	331 776	$L_1^0(18, 20)$	160 432 128
$L_1^0(4, 8)$	45 792	$L_1^0(10, 14)$	52 862 976	$L_1^0(18, 22)$	75 497 472 000
$L_1^0(4, 10)$	645 120	$L_1^0(10, 16)$	6 258 180 096	$L_1^0(18, 24)$	2.36626×10^{13}
$L_1^0(4, 12)$	-26 224 128	$L_1^0(10, 18)$	5.99330×10^{11}	$L_1^0(18, 26)$	5.50232×10^{15}
$L_1^0(4, 14)$	-3 201 067 008	$L_1^0(10, 20)$	4.87727×10^{13}	$L_1^0(18, 28)$	1.01809×10^{18}
$L_1^0(4, 16)$	-2.14087×10^{11}	$L_1^0(10, 22)$	3.47446×10^{15}	$L_1^0(18, 30)$	1.57315×10^{20}
$L_1^0(4, 18)$	-1.19007×10^{13}	$L_1^0(10, 24)$	2.20156×10^{17}	$L_1^0(20, 20)$	629 145.6
$L_1^0(4, 20)$	-6.00757×10^{14}	$L_1^0(10, 26)$	1.24531×10^{19}	$L_1^0(20, 22)$	717 225 984
$L_1^0(4, 22)$	-2.84486×10^{16}	$L_1^0(10, 28)$	6.20798×10^{20}	$L_1^0(20, 24)$	4.11140×10^{11}
$L_1^0(4, 24)$	-1.28105×10^{18}	$L_1^0(10, 30)$	2.59861×10^{22}	$L_1^0(20, 26)$	1.54445×10^{14}
$L_1^0(4, 26)$	-5.50874×10^{19}	$L_1^0(12, 12)$	4 096	$L_1^0(20, 28)$	4.24543×10^{16}
$L_1^0(4, 28)$	-2.25576×10^{21}	$L_1^0(12, 14)$	1 622 016	$L_1^0(20, 30)$	9.17892×10^{18}
$L_1^0(4, 30)$	-8.69402×10^{22}	$L_1^0(12, 16)$	360 603 648	$L_1^0(22, 22)$	2 287 802.18
$L_1^0(6, 6)$	128	$L_1^0(12, 18)$	57 416 810 496	$L_1^0(22, 24)$	3 170 893 824
$L_1^0(6, 8)$	11 520	$L_1^0(12, 20)$	7.19497×10^{12}	$L_1^0(22, 26)$	2.17478×10^{12}
$L_1^0(6, 10)$	716 544	$L_1^0(12, 22)$	7.51820×10^{14}	$L_1^0(22, 28)$	9.64167×10^{14}
$L_1^0(6, 12)$	35 891 712	$L_1^0(12, 24)$	6.80443×10^{16}	$L_1^0(22, 30)$	3.09123×10^{17}
$L_1^0(6, 14)$	1 464 910 848	$L_1^0(12, 26)$	5.46987×10^{18}	$L_1^0(24, 24)$	8 388 608
$L_1^0(6, 16)$	43 817 011 200	$L_1^0(12, 28)$	3.96931×10^{20}	$L_1^0(24, 26)$	13 891 534 848
$L_1^0(6, 18)$	3.17933×10^{11}	$L_1^0(12, 30)$	2.62442×10^{22}	$L_1^0(24, 28)$	1.12307×10^{13}
$L_1^0(6, 20)$	-8.54676×10^{13}	$L_1^0(14, 14)$	14 043.43	$L_1^0(24, 30)$	5.80075×10^{15}
$L_1^0(6, 22)$	-9.18906×10^{15}	$L_1^0(14, 16)$	7 667 712	$L_1^0(26, 26)$	30 973 321.85
$L_1^0(6, 24)$	-6.76634×10^{17}	$L_1^0(14, 18)$	2 263 154 688	$L_1^0(26, 28)$	60 397 977 600
$L_1^0(6, 26)$	-4.25366×10^{19}	$L_1^0(14, 20)$	4.64539×10^{11}	$L_1^0(28, 28)$	115 043 766.9
$L_1^0(6, 28)$	-2.43350×10^{21}	$L_1^0(14, 22)$	7.33145×10^{13}	$L_1^0(28, 30)$	2.60919×10^{11}
$L_1^0(6, 30)$	-1.30192×10^{23}	$L_1^0(14, 24)$	9.47783×10^{15}	$L_1^0(30, 30)$	429 496 729.6
$L_1^0(8, 8)$	384	$L_1^0(14, 26)$	1.04744×10^{18}	$L_1^0(8, n) = -L_2^0(4, n)$ $L_1^0(12, n) = -L_2^0(6, n) = L_3^0(4, n)$ $L_1^0(16, n) = -L_2^0(8, n) = -L_4^0(4, n)$ $L_1^0(18, n) = L_3^0(6, n)$ $L_1^0(20, n) = -L_2^0(10, n) = L_5^0(4, n)$ $L_1^0(24, n) = -L_2^0(12, n) = L_3^0(8, n)$ $\quad = -L_4^0(6, n) = -L_6^0(4, n)$ $L_1^0(28, n) = -L_2^0(14, n) = L_7^0(4, n)$ $L_1^0(30, n) = L_3^0(10, n) = L_5^0(6, n)$	
$L_1^0(8, 10)$	64 512	$L_1^0(14, 28)$	1.01916×10^{20}		
$L_1^0(8, 12)$	6 842 880	$L_1^0(14, 30)$	8.91247×10^{21}		
$L_1^0(8, 14)$	563 816 448	$L_1^0(16, 16)$	49 152		
$L_1^0(8, 16)$	38 644 455 168	$L_1^0(16, 18)$	35 389 440		
$L_1^0(8, 18)$	2.27266×10^{12}	$L_1^0(16, 20)$	13 373 669 376		
$L_1^0(8, 20)$	1.15216×10^{14}	$L_1^0(16, 22)$	3.43220×10^{12}		
$L_1^0(8, 22)$	4.87450×10^{15}	$L_1^0(16, 24)$	6.64230×10^{14}		
$L_1^0(8, 24)$	1.48769×10^{17}	$L_1^0(16, 26)$	1.03670×10^{17}		
$L_1^0(8, 26)$	3.87212×10^{17}	$L_1^0(16, 28)$	1.36624×10^{19}		
$L_1^0(8, 28)$	-4.23050×10^{20}	$L_1^0(16, 30)$	1.57009×10^{21}		
$L_1^0(8, 30)$	-4.60409×10^{22}				

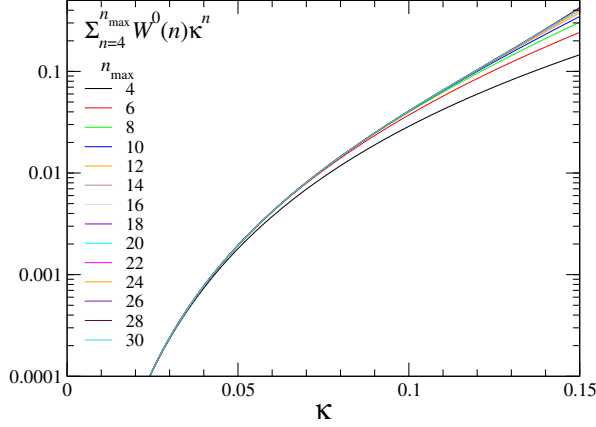


Fig. 3 n_{\max} dependence of $\sum_{n=4}^{n_{\max}} W^0(n) \kappa^n$ for the case $U_{x,\mu} = 1$. The vertical axis is in a logarithmic scale.

4 Effect of high order terms

Though the convergence radius of the hopping parameter expansion turned out to be not small, in practice, we need to truncate the expansion at some finite order and have to take into account the systematic error due to the truncation. In this section, we study the effect of higher-order terms more closely and estimate the magnitude of the truncation error considering the case of the worst convergence. We also introduce an effective theory to incorporate the effect of high order term to reduce the truncation error of the hopping parameter expansion.

From Eq. (5), the expectation value at the simulation point (β, κ) can be expressed in terms of those at a different simulation point (β_0, κ_0) by the reweighting method [1]:

$$\langle \mathcal{O} \rangle_{(\beta, \kappa)} = \frac{\langle \mathcal{O} [\det M(\kappa) / \det M(\kappa_0)]^{N_f} e^{6(\beta - \beta_0) N_{\text{site}} \hat{P}} \rangle_{(\beta_0, \kappa_0)}}{\langle [\det M(\kappa) / \det M(\kappa_0)]^{N_f} e^{6(\beta - \beta_0) N_{\text{site}} \hat{P}} \rangle_{(\beta_0, \kappa_0)}}. \quad (45)$$

Setting $\kappa_0 = 0$, we find from Eqs. (6) and (9) that the hopping parameter expansion of the reweighting factor is given by

$$\det M(\kappa) = \exp \left[N_{\text{site}} \sum_{n=4}^{\infty} W(n) \kappa^n + N_{\text{site}} \sum_{n=N_t}^{\infty} \sum_{m=1}^{\infty} L_m(N_t, n) \kappa^n \right]. \quad (46)$$

4.1 Effect of Wilson loop terms

We first discuss the effect of the Wilson loop terms, $\sum_{n=4}^{\infty} W(n) \kappa^n$, in Eq. (46). In practice, we need to truncate the hopping parameter expansion by introducing a highest power of κ , say n_{\max} . To see an upper bound for the truncation error of the hopping parameter expansion, we study the case of worst convergence $U_{x,\mu} = 1$ discussed in Sec. 3. Using the results of Table 1, we compute $\sum_{n=4}^{n_{\max}} W^0(n) \kappa^n$ as functions of κ . The results are shown in Fig. 3 for $n_{\max} = 4$ –30. We see that the truncation error in the sum of Wilson loop terms is small up to $\kappa \simeq 0.125$ when we choose $n_{\max} \gtrsim 10$.

Next, we discuss the effect of each Wilson loop term $W(n)$. Since the first term $W(4)$ is proportional to \hat{P} , its effects can be reproduced by a shift $\beta \rightarrow \beta^* = \beta + 48N_f\kappa^4$ in the gauge action. Though Wilson loops of $n \geq 6$ do not appear in the standard plaquette gauge action, they can also be regarded as lattice expression of the gauge action. In fact, improved gauge actions contain terms with such longer Wilson loops. Therefore, the effect of the Wilson loop terms can be reproduced by the following modification of the lattice gauge action,

$$\begin{aligned} 6\beta\hat{P} &\longrightarrow 6\beta\hat{P} + N_f[W(4)\kappa^4 + W(6)\kappa^6 + W(8)\kappa^8 + W(10)\kappa^{10} + \dots] \\ &= 6(\beta + 48N_f\kappa^4)\hat{P} + N_f[8448\kappa^6\hat{P}_6 + 245952\kappa^8\hat{P}_8 + 7372800\kappa^{10}\hat{P}_{10} + \dots], \end{aligned} \quad (47)$$

where, \hat{P}_n is the linear combination of n -step Wilson loops in $W(n)$ and is normalized to one when $U_{x,\mu} = \mathbf{1}$. When we view this shift of the gauge action as a shift in improvement parameters in the parameter space of improved gauge actions, we find that, at least in these low-order terms, the magnitude of the shift is much smaller than those for typical improved actions: For example, in the Iwasaki improved gauge action, $S_g = -6N_{\text{site}}\beta(c_0\hat{P} + 2c_1\hat{R})$ with \hat{R} the 1×2 Wilson loop, the improvement parameters are $c_0 = 3.648$ and $c_1 = -0.331$, i.e., the ratio of the absolute values of the 4-step and 6-step terms is about $5.5 : 1$ [13]. On the other hand, the ratio of the 4-step term to the 6-step term in Eq. (47) is about $4000 : N_f$ even at $\kappa \sim 0.1$. The magnitude of coupling parameters is similar also in other improved gauge actions [14–16]. Therefore, the shift in gauge coupling parameters due to the dynamical quark effect is quite small at $\kappa \lesssim 0.1$.¹ Because a slight shift in improvement parameters mainly affects the lattice discretization errors, the Wilson loop terms will not affect characteristic features of the system in the continuum limit, though the convergence of the hopping parameter expansion may rapidly worsen close to the chiral limit. In contrast, the Polyakov-type loop terms affect like external magnetic fields in spin models, and thus can change the nature of the phase transition.

4.2 Truncation error of higher-order Polyakov-type loop terms

We now study the effect of Polyakov-type loop terms. To see an upper bound for the truncation error of the hopping parameter expansion, we first study the case of worst convergence, $U_{x,\mu} = \mathbf{1}$, discussed in Sec. 3:

$$[\ln \det M(\kappa) - (\text{Wilson loop terms})]_{U_{x,\mu}=\mathbf{1}} \simeq N_{\text{site}} \sum_{n=N_t}^{n_{\text{max}}} L^0(N_t, n) \kappa^n, \quad (48)$$

where n_{max} is the highest power of κ to truncate the hopping parameter expansion. In Figs. 4 and 5, we plot $\sum_{n=N_t}^{n_{\text{max}}} L^0(N_t, n) \kappa^n$ changing $n_{\text{max}} = N_t, N_t + 2, \dots$ up to 30 on $N_t = 4$ –14 lattices.

The left panel of Fig. 4 shows the results for $N_t = 4$. The vertical dashed line represents $\kappa_c = 0.0602(4)$ for two-flavor QCD [8], which was obtained for infinitely large spatial volume by a finite size scaling analysis including the next-to-leading order effect, i.e., $n_{\text{max}} = N_t + 2$. The location of the critical point for three-flavor QCD is similar [5, 8]. From this plot, we see that, around κ_c of two- and three-flavor QCD, the κ^4 term is dominant and the effect of the higher-order terms is

¹ We also note that, since the sign of the 6-step loop term of typical improved actions is negative while that of the $W(6)$ term is positive, a slight unimprovement is required to reproduce the dynamic quark effect.

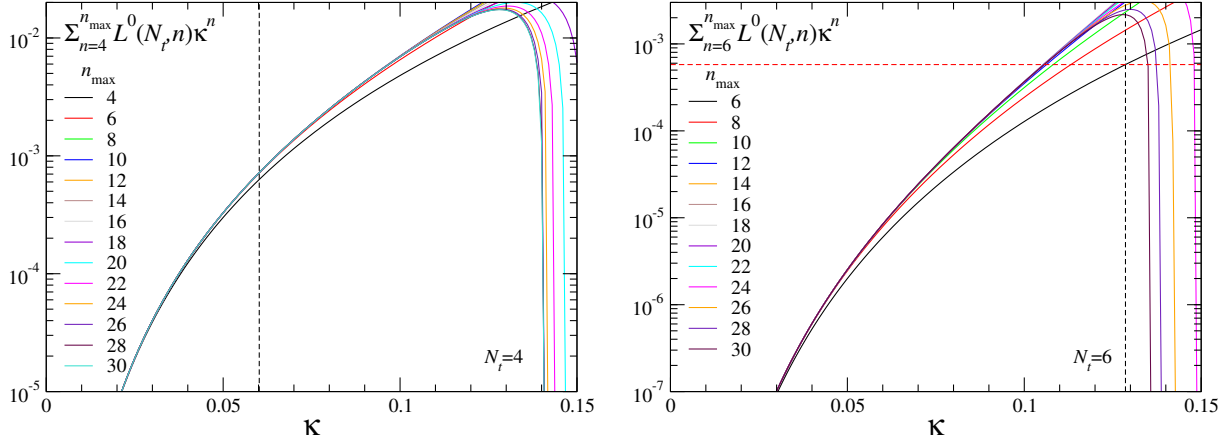


Fig. 4 n_{\max} dependence of $\sum_{n=N_t}^{n_{\max}} L^0(N_t, n) \kappa^n$ at $N_t = 4$ (left) and $N_t = 6$ (right) for the case $U_{x,\mu} = 1$.

negligible. Hence, the determination of κ_c using the hopping parameter expansion is reliable for $N_t = 4$. We also see that the convergence of the hopping parameter expansion suddenly worsens at $\kappa \gtrsim 0.13$, suggesting a lower bound of the convergence radius around there.

In the right panel of Fig. 4, we show the corresponding results for $N_t = 6$. The vertical dashed line shows the critical point $\kappa_c = 0.1286(40)$ for two-flavor QCD obtained by looking at the shape of the histogram of the Polyakov loop on a $32^3 \times 6$ lattice [7], which was calculated with the leading-order term, i.e., $n_{\max} = N_t$. Here, we notice that the critical point determined by the histogram has a large systematic error due to the finite volume effect. The critical point determined by the histogram is about 10% larger than that determined by a finite size scaling analysis on $N_t = 4$ lattices [8]. From a full QCD simulation on $N_t = 6$ lattices, $\kappa_c = 0.0877(9)$ is obtained by a finite size scaling analysis [11].

Unlike the case of $N_t = 4$ shown in the left panel of Fig. 4, we see significant effect from high order terms for $N_t = 6$ around κ_c determined on a $32^3 \times 6$ lattice by a leading-order calculation. The results for $N_t = 8, 10, 12$, and 14 are shown in Fig. 5. We see that the convergence worsens further as N_t increases. Note, however, that these results are obtained for the case $U_{x,\mu} = 1$. As discussed in Sec. 3, because the values of Polyakov loops on actual configurations become exponentially small as n increases, the convergence in actual simulations should be better than the case $U_{x,\mu} = 1$. In the next subsection, we also discuss that the convergence is much improved by incorporating higher-order effects — using an effective theory incorporating high order terms, we can reliably determine the critical point κ_c for the case of $N_t = 6$.

4.3 Effective theory incorporating high order terms

As noted in Refs. [6, 7], the Polyakov loop $\hat{\Omega}$ and the bent Polyakov loops $\hat{\Omega}_k$ are strongly correlated on each configuration. In Ref. [7], this correlation was used to construct an effective theory in which the next-to-leading order effect of $\hat{\Omega}_k$ is effectively absorbed into a shift of the coupling for the leading order term $\hat{\Omega}$. In Sec. 5, we show more generally that $L(N_t, n)$ and $\hat{\Omega}$ are

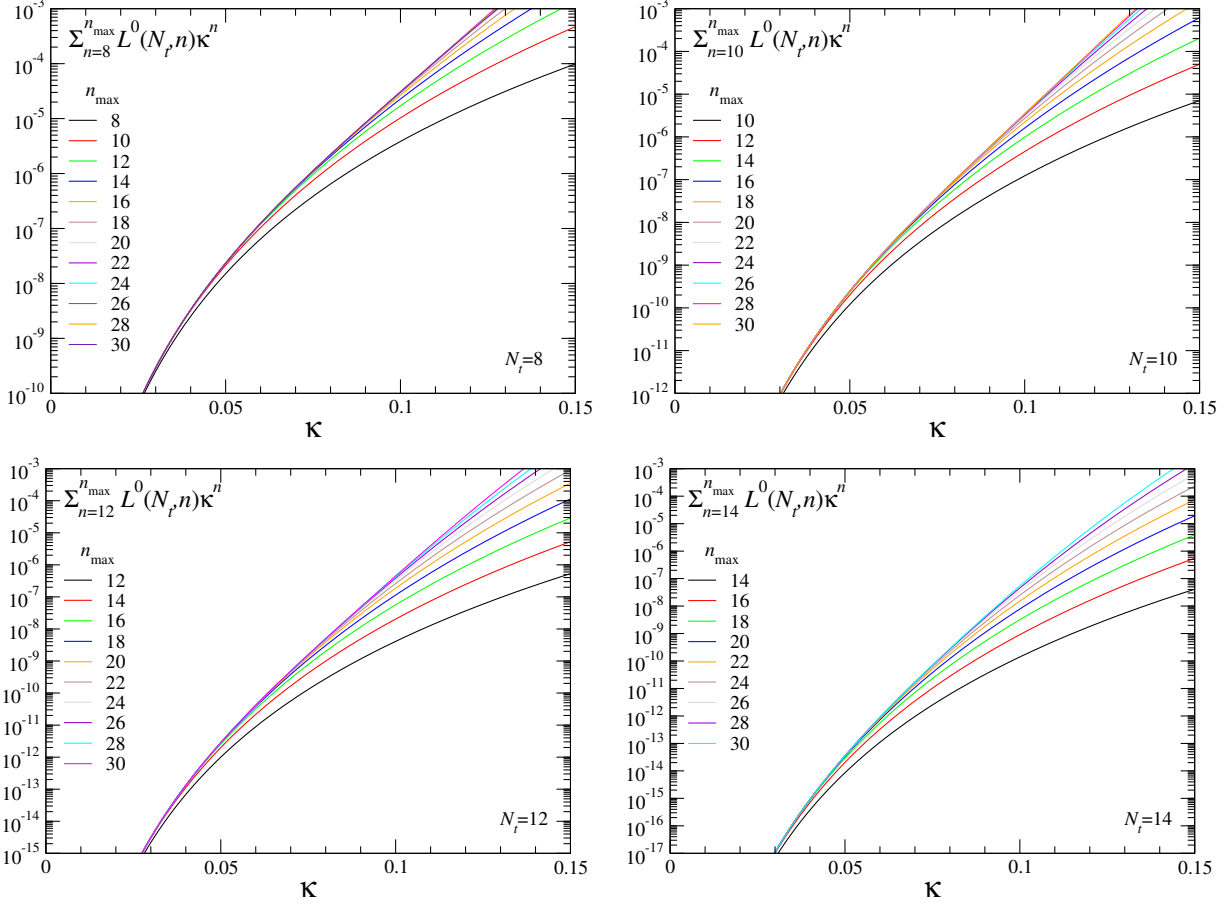


Fig. 5 The same as Fig. 4, but for $N_t = 8$ (top left), 10 (top right), 12 (bottom left), and 14 (bottom right).

strongly correlated with each other on each configuration. We may thus approximate $L(N_t, n)$ by

$$L(N_t, n) \approx L^0(N_t, n) c_n \text{Re}\hat{\Omega}, \quad (49)$$

where c_n is a constant to be determined by measuring the correlation between $L(N_t, n)$ and $\hat{\Omega}$ by a Monte Carlo simulation at each simulation point, while $c_n = 1$ for $n = N_t$, and $c_n = 0$ if n is odd or $n < N_t$. We have $c_{N_t+2} = 0.7996(7)$ around the phase transition point for $N_t = 4$, and $0.8130(3)$ for $N_t = 6$ [7]. In Sec. 5, we determine c_n up to $n = 20$ around the phase transition point for $N_t = 6$ and 8.

From Eq. (49), the Polyakov-type loop terms in the effective quark action $\ln \det M(\kappa)$ are approximated as

$$\sum_{n=N_t}^{n_{\max}} L(N_t, n) \kappa^n \approx \left[\sum_{n=N_t}^{n_{\max}} L^0(N_t, n) c_n \kappa^n \right] \text{Re}\hat{\Omega}. \quad (50)$$

Equation (50) means that the effect of high order Polyakov-type loop terms can be effectively incorporated to the leading order calculation by a shift of κ appearing in front of $\text{Re}\hat{\Omega}$ of the

leading-order correction term:

$$L^0(N_t, N_t) \kappa^{N_t} \longrightarrow L^0(N_t, N_t) (\kappa^*)^{N_t} = \sum_{n=N_t}^{n_{\max}} L^0(N_t, n) c_n \kappa^n \quad (51)$$

in the leading order calculation. For example, when the critical point is determined as $\kappa_{c,\text{LO}}$ by a leading-order calculation, then we obtain the critical point $\kappa_{c,\text{eff}}$ effectively incorporating higher-order effects up to n_{\max} -th order by solving

$$\sum_{n=N_t}^{n_{\max}} L^0(N_t, n) c_n \kappa_{c,\text{eff}}^n = L^0(N_t, N_t) \kappa_{c,\text{LO}}^{N_t}. \quad (52)$$

We now revisit the case of worst convergence discussed in Sec. 4.2. In the right panel of Fig. 4, $L^0(N_t, N_t) \kappa_{c,\text{LO}}^{N_t}$ for $N_t = 6$ is shown by the red dashed line. The colored solid lines represent the left-hand-side of Eq. (52) for various n_{\max} with substituting $c_n = 1$. The red dashed line intersects each colored solid line at $\kappa = \kappa_{c,\text{eff}}$ for the corresponding n_{\max} . From the right panel of Fig. 4, we find that, even in the case of worst convergence with $c_n = 1$, a stable and reliable $\kappa_{c,\text{eff}}$ is obtained for $N_t = 6$ when $n_{\max} \gtrsim 10$. Since $c_n < 1$ in practice, the correction of $\kappa_{c,\text{eff}}$ from higher-order terms is smaller than the case of $c_n = 1$ shown in Fig. 4. Thus the next-to-leading order calculation of $\kappa_{c,\text{eff}}$ for $N_t = 6$ with $n_{\max} = 8$ [7] may not be so wrong.

For $N_t = 8$, though $\kappa_{c,\text{LO}}$ is not available yet², the top left panel of Fig. 5 shows that higher-order effects are well suppressed up to $\kappa \lesssim 0.125$ when we choose $n_{\max} \gtrsim 20$. As N_t increases, the convergence gradually worsens and thus a larger value of n_{\max} will be required to obtain a reliable κ_c by the hopping parameter expansion.

5 Correlation among expansion terms

5.1 Calculation of expansion terms by numerical simulation

We now perform Monte Carlo simulations of $SU(3)$ lattice gauge theory (quenched QCD) around the phase transition point to calculate the expansion terms $W(n)$ and $L_m(N_t, n)$ and study correlations among them. As discussed in Sec. 2, $W(n)$ and $L_m(N_t, n)$ can be extracted by calculating $D_n = (-1/N_{\text{site}}n) \text{Tr}[B^n]$ defined by Eq. (8) with various boundary conditions.

To calculate D_n , we adopt the noise method for the trace over the position index: For each of the i -th set of the 3×4 color and spinor indexes, we generate a series of random numbers $(\vec{\eta}_j)_x$ with random complex phase at each position x , where the random vectors $\vec{\eta}_j$ satisfy

$$\lim_{N_{\text{noise}} \rightarrow \infty} \frac{1}{N_{\text{noise}}} \sum_{j=1}^{N_{\text{noise}}} (\vec{\eta}_j^*)_y (\vec{\eta}_j)_x = \delta_{y,x}. \quad (53)$$

Multiplying B^n to $\vec{\eta}_j$ and calculating the inner product with the complex conjugate $\vec{\eta}_j^*$ of the original vector, we obtain $\text{Tr}[B^n]$ as

$$\lim_{N_{\text{noise}} \rightarrow \infty} \frac{1}{N_{\text{noise}}} \sum_{j=1}^{N_{\text{noise}}} \sum_i \sum_{x,y} (\vec{\eta}_j^*)_y [B^n]_{ii,yx} (\vec{\eta}_j)_x = \sum_i \sum_x [B^n]_{ii,xx} = \text{Tr}[B^n] \quad (54)$$

² $\kappa_c = 0.1135(8)$ was reported for $N_t = 8$ by a full QCD simulation of Ref. [11].

We calculate D_n with the following four types of boundary conditions in the temporal direction, while we impose periodic boundary condition in the spatial directions. D_n for periodic and anti-periodic boundary conditions are given by Eqs. (16) and (9), respectively. Next, we prepare a lattice with a size of $N_s^3 \times (2N_t)$ by copying configurations generated on the $N_s^3 \times N_t$ lattice twice along the temporal direction. Since Polyakov-type loops do not close for $n < 2N_t$ on this lattice, D_n in this case with periodic boundary condition D_n^{2+} and anti-periodic boundary condition D_n^{2-} are given by

$$D_n^{2+} = W(n) + \sum_{m=1}^{\infty} L_{2m}(N_t, n) = \frac{D_n + D_n^+}{2}, \quad (55)$$

$$D_n^{2-} = W(n) + \sum_{m=1}^{\infty} (-1)^m L_{2m}(N_t, n) = \frac{D_n^i + D_n^{-i}}{2}, \quad (56)$$

respectively. These relations lead

$$(D_n + D_n^+ + 2D_n^{2-})/4 = W(n) + L_4(N_t, n) + \cdots, \quad (57)$$

$$(D_n + D_n^+ - 2D_n^{2-})/4 = L_2(N_t, n) + L_6(N_t, n) + \cdots, \quad (58)$$

$$(D_n - D_n^+)/2 = L_1(N_t, n) + L_3(N_t, n) + L_5(N_t, n) + \cdots. \quad (59)$$

Using these relations, we calculate $W(n)$ etc. for $n < 4N_t$. As discussed in Sec. 4.3, to determine κ_c for $N_t = 8$, a calculation up to about $O(\kappa^{20})$ may be required. We thus calculate $L_m(N_t, n)$ for n from N_t up to 20. For $n \leq 20$, because $L_m(6, n) = 0$ for $m \geq 4$ and $L_m(8, n) = 0$ for $m \geq 3$, we have $W(n) = (D_n + D_n^+ + 2D_n^{2-})/4$, $L_1(N_t, n) + L_3(N_t, n) = (D_n - D_n^+)/2$, $L_2(N_t, n) = (D_n + D_n^+ - 2D_n^{2-})/4$, and $L(N_t, n) = L_1(N_t, n) + L_2(N_t, n) + L_3(N_t, n)$. We thus compute D_n , D_n^+ and D_n^{2-} .

We perform simulations on a $32^3 \times 6$ lattice at $\beta = 5.8810$ and 5.9000 , and on a $32^3 \times 8$ lattice at $\beta = 6.0320$ and 6.0660 . These β values are chosen to be slightly below and above the phase transition point.³ Details of the simulations are the same as in our previous studies [5–7, 9, 10]. Independent 50 configurations are generated at each β . The number of noises N_{noise} is 1000 for each configuration.

5.2 Correlation among Polyakov-type loop terms

In Fig. 6, we plot the double distribution of $L(N_t, n)/L^0(N_t, n)$ (vertical axis) and $\text{Re}\hat{\Omega} = L(N_t, N_t)/L^0(N_t, N_t)$ (horizontal axis) obtained on each configuration of the $N_t = 6$ lattice. The blue and red symbols are for $\beta = 5.8810$ and 5.9000 , respectively. The error bar represents the error caused by the finite N_{noise} on each configuration, which decreases as n increases since $L(N_t, n)/L^0(N_t, n)$ is a weighted average of Polyakov-type loops and the number of Polyakov-type loops to be averaged increases as n increases. Although the results of these figures include contributions from $L_1(N_t, n)$, $L_2(N_t, n)$ and $L_3(N_t, n)$, the contributions from $L_2(N_t, n)$ and $L_3(N_t, n)$ are negligibly small compared to $L_1(N_t, n)$. The top left panel of Fig. 6 shows the result of $n = 6$.

³ The transition point determined by the peak of the Polyakov loop susceptibility locates at $\beta_{\text{trans}} = 5.89383(24)$ on a $48^3 \times 6$ lattice and at $6.06160(18)$ on a $48^3 \times 8$ lattice [17].

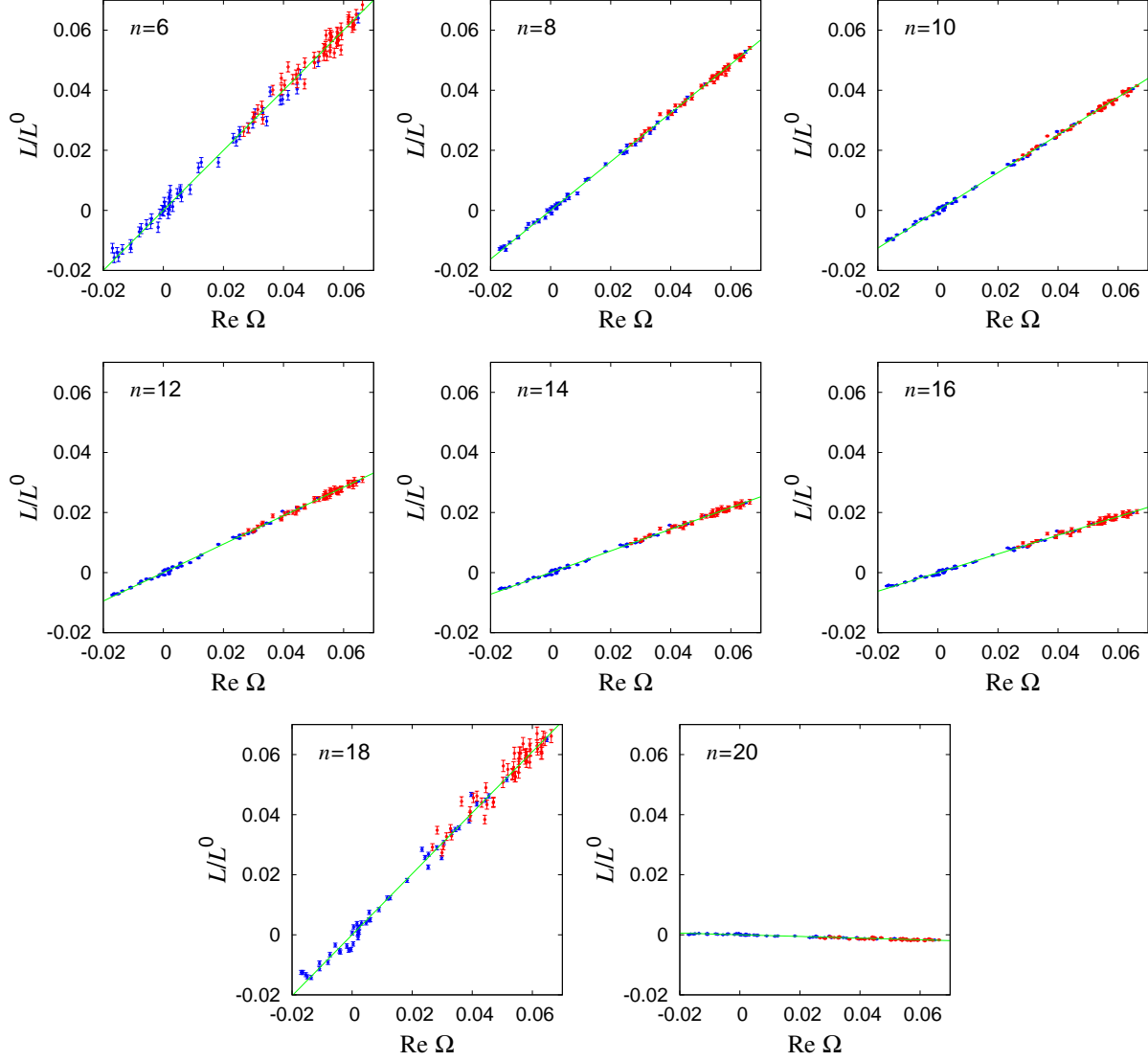


Fig. 6 Double distribution of $L(N_t, n)/L^0(N_t, n)$ and $\text{Re}\hat{\Omega}$ obtained on $32^3 \times 6$ lattice. The top left, top middle, \dots , and bottom right panels show the results of $n = 6, 8, \dots$, and 20, respectively. The blue and red symbols are the results obtained at $\beta = 5.8810$ and 5.9000 , respectively. The green lines are the results of linear fits with Eq. (49). As discussed in the text, the cases $n = 18$ and 20 are a little special because $L^0(N_t, n)$ in the denominator changes sign between $n = 18$ and 20.

Because $L(6, 6) = L^0(6, 6) \text{Re}\hat{\Omega}$, both axes are $\text{Re}\hat{\Omega}$, and the figure confirms the accuracy of the noise method. The other panels are the results of $n = 8$ (top middle), 10 (top right), 12 (middle left), 14 (middle), 16 (middle right), 18 (bottom left), and 20 (bottom right).

Figure 7 shows the double distribution of $L(N_t, n)/L^0(N_t, n)$ and $\text{Re}\hat{\Omega}$ obtained on the $N_t = 8$ lattice. Each panel shows the result for $n = 10$ (top left), 12 (top middle), 14 (top right), 16 (bottom

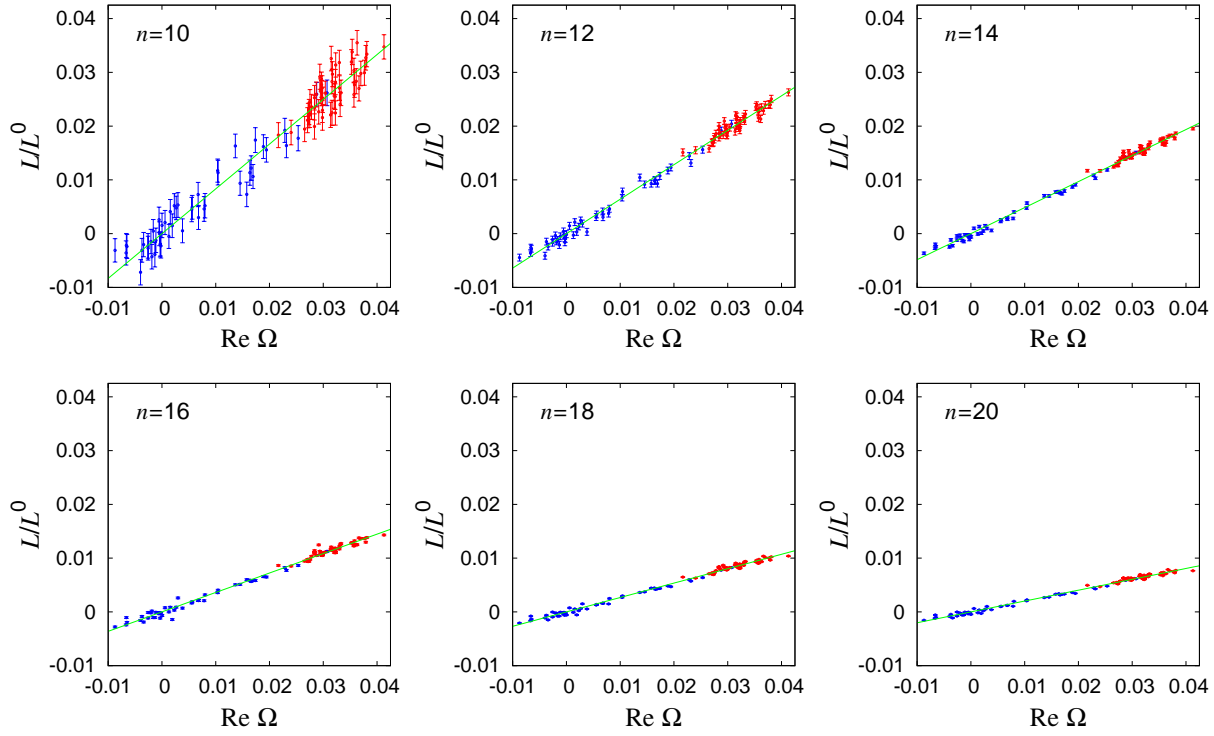


Fig. 7 The same as Fig. 6 but on $32^3 \times 8$ lattice at $\beta = 6.0320$ (blue) and 6.0660 (red). The top left, top middle, \dots , and bottom right panels show the results of $n = 10, 12, \dots$, and 20 , respectively.

Table 3 Coefficients c_n of Eq. (49) for $n = N_t - 20$ on $N_t = 6$ and 8 lattices.

	$N_t = 6$	$N_t = 8$
c_6	1	
c_8	0.8112(20)(7)	1
c_{10}	0.6280(15)(3)	0.8327(114)(95)
c_{12}	0.4736(29)(15)	0.6408(36)(27)
c_{14}	0.3609(26)(11)	0.4841(22)(10)
c_{16}	0.3106(25)(10)	0.3616(21)(6)
c_{18}	1.0159(90)(33)	0.2679(16)(3)
c_{20}	-0.02771(57)(13)	0.2020(13)(2)

left), 18 (bottom middle) and 20 (bottom right), respectively, obtained at $\beta = 6.0320$ (blue) and 6.0660 (red).

These figures show that $L(N_t, n)$ has a strong linear correlation with $\text{Re}\hat{\Omega}$, i.e., Eq. (49) is well satisfied. We thus calculate the coefficient c_n by fitting the $L(N_t, n)$ data by Eq. (49), for each n

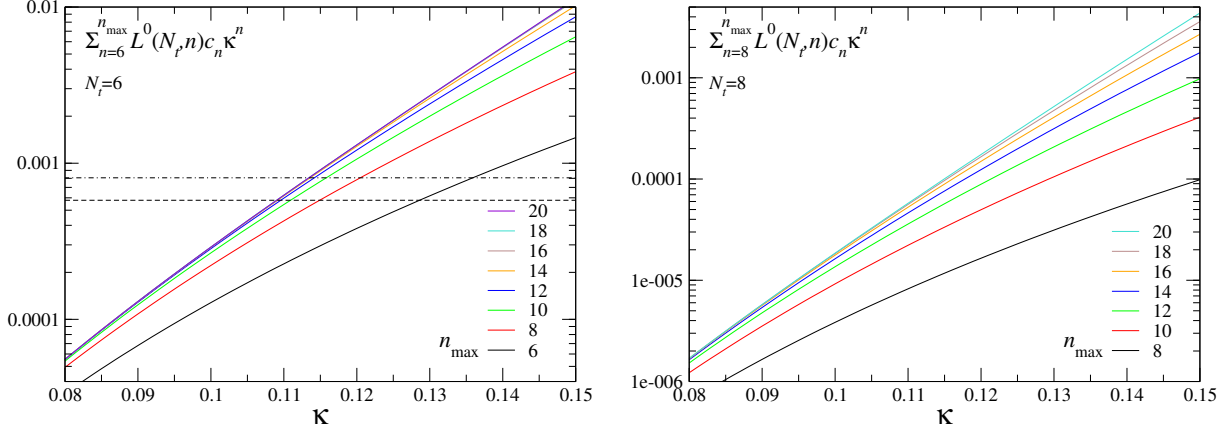


Fig. 8 $\sum_{n=N_t}^{n_{\max}} L^0(N_t, n) c_n \kappa^n$ for $N_t = 6$ (left) and 8 (right) as functions of n_{\max} . The horizontal dot-dashed and dashed lines in the left panel are $L^0(N_t, N_t) \kappa_{c, \text{LO}}^{N_t}$ obtained on $24^3 \times 6$ and $32^3 \times 6$ lattices, respectively.

Table 4 Effective critical point $\kappa_{c, \text{eff}}$ in degenerate N_f -flavor QCD on $N_t = 6$ lattice.

$N_s^3 \times N_t$	$N_f = 1$	$N_f = 2$	$N_f = 3$
$24^3 \times 6$	0.1228(18)	0.1134(18)	0.1080(17)
$32^3 \times 6$	0.1183(25)	0.1090(25)	0.1037(24)

and N_t . Minimizing $\chi^2 = \sum_i [(L(i) - L^0(N_t, n) c_n \text{Re}\hat{\Omega}(i)) / \Delta L(i)]^2$, with $L(i)$ the result of $L(N_t, n)$ on the i -th configuration and $\Delta L(i)$ the error of $L(i)$ due to the noise method, the best value of c_n is given by

$$c_n = \frac{1}{L^0(N_t, n)} \frac{\langle L(N_t, n) \text{Re}\hat{\Omega} / \Delta L^2 \rangle}{\langle (\text{Re}\hat{\Omega})^2 / \Delta L^2 \rangle}. \quad (60)$$

The error propagation from ΔL to c_n is given by

$$\Delta c_n = \frac{1}{\sqrt{N_{\text{conf}}} |L^0(N_t, n)|} \left\langle \frac{(\text{Re}\hat{\Omega})^2}{\Delta L^2} \right\rangle^{-1/2},$$

where N_{conf} is the number of configurations.

The results of the fits are shown by the green lines in Figs. 6 and 7. We summarize the results of c_n in Table 3, in which the numbers in the first parenthesis are the statistical errors and those in the second parenthesis are the errors propagated from the error of the noise method. We note that c_n decreases by a factor of about 0.8 as the order of κ^2 increases by one. Thus, our results of c_n are well approximated by $c_n \approx (0.8)^{(n-N_t)/2}$, except for c_{18} and c_{20} for $N_t = 6$ — the cases $n = 18$ and 20 for $N_t = 6$ are a little special because the sign of $L^0(N_t, n)$ changes between 18 and 20 and thus the positive sign terms and the negative sign terms cancel with each other in $L^0(N_t, n)$ there. For $N_t = 8$, the sign of $L^0(N_t, n)$ changes first at $n = 28$.

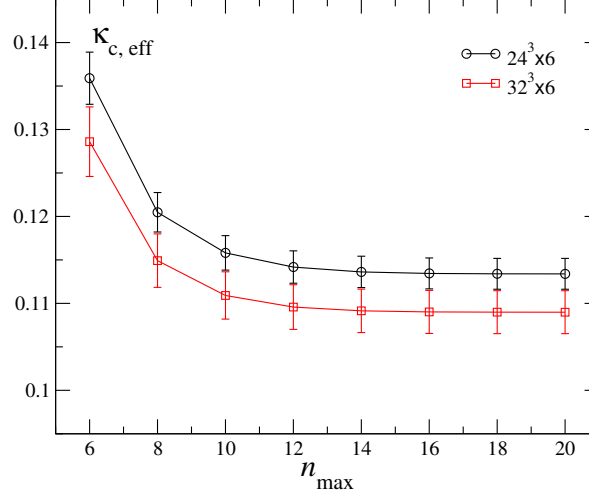


Fig. 9 Effective critical point $\kappa_{c,\text{eff}}$ in two flavor QCD for $N_t = 6$ as function of n_{\max} . Black circle and red square symbols are for the results using $\kappa_{c,\text{LO}}$ obtained on $24^3 \times 6$ and $32^3 \times 6$ lattices, respectively.

5.3 Location of critical point incorporating high order effects

We now determine the effective critical point $\kappa_{c,\text{eff}}$ by substituting c_n of Table 3 into Eq. (52), i.e.,

$$\sum_{n=N_t}^{n_{\max}} L^0(N_t, n) c_n \kappa_{c,\text{eff}}^n = L^0(N_t, N_t) \kappa_{c,\text{LO}}^{N_t}.$$

In Fig. 8, we show $\sum_{n=N_t}^{n_{\max}} L^0(N_t, n) c_n \kappa^n$ for $N_t = 6$ (left panel) and 8 (right panel) using c_n of Table 3. For $\kappa_{c,\text{LO}}$ in the right hand side of Eq. (52), we adopt the results of leading-order calculation in two flavor QCD, $\kappa_{c,\text{LO}} = 0.1359(30)$ obtained on a $24^3 \times 6$ lattice, and also $\kappa_{c,\text{LO}} = 0.1286(40)$ obtained on a $32^3 \times 6$ lattice [7]. In the left panel, the horizontal dot-dashed and dashed lines are the $L^0(N_t, N_t) \kappa_{c,\text{LO}}^{N_t}$ obtained on $24^3 \times 6$ and $32^3 \times 6$ lattices, respectively. The crossing points of the horizontal line with colored solid curves give the values of the effective critical point $\kappa_{c,\text{eff}}$ for various n_{\max} .

In Fig. 9, we show the results of $\kappa_{c,\text{eff}}$ for $N_t = 6$ as function of n_{\max} . Black and red data are obtained using $\kappa_{c,\text{LO}}$ on $24^3 \times 6$ and $32^3 \times 6$ lattices, respectively. Our result $\kappa_{c,\text{eff}} = 0.1205(23)$ for $n_{\max} = N_t + 2$ on the $24^3 \times 6$ lattice is consistent with the result of the next-to-leading-order calculation given in Ref. [7]. As n_{\max} increases, $\kappa_{c,\text{eff}}$ converges to $\kappa_{c,\text{eff}} = 0.1134(18)$ for the $24^3 \times 6$ lattice and $0.1090(25)$ for $32^3 \times 6$. We find that the hopping parameter expansion works well for $N_t = 6$ when high order effects are incorporated up to a sufficiently high order. At the same time, we note sizable finite volume effect in $\kappa_{c,\text{eff}}$. Large finite volume effect was reported also in the leading-order determination of the critical point by the shape of the histogram of the Polyakov loop [8]. It is important to perform a systematic study with large spatial volumes to remove the finite volume effect.

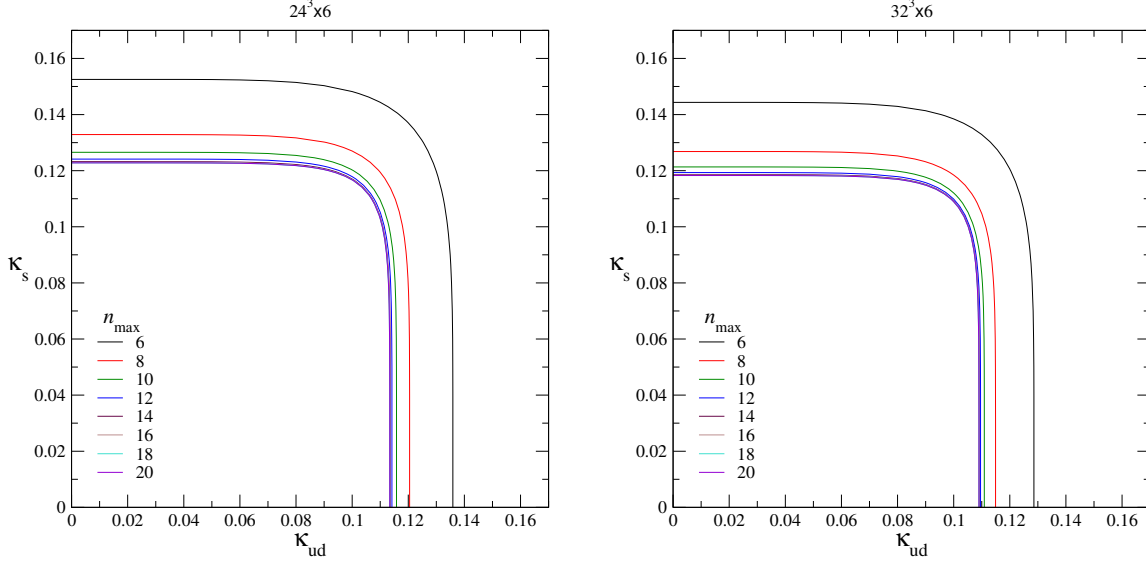


Fig. 10 Critical line in 2+1-flavor QCD calculated with various n_{\max} for $24^3 \times 6$ (left) and $32^3 \times 6$ (right) lattices.

It is easy to generalize the argument to the case of non-degenerate quarks. For 2+1-flavor QCD, denoting the hopping parameter for the up and down quarks as κ_{ud} and that for the strange quark as κ_s , the critical line in the (κ_{ud}, κ_s) plane is obtained by finding $(\kappa_{c,ud}, \kappa_{c,s})$ that satisfies the following equation

$$2 \sum_{n=N_t}^{n_{\max}} L^0(N_t, n) c_n \kappa_{c,ud}^n + \sum_{n=N_t}^{n_{\max}} L^0(N_t, n) c_n \kappa_{c,s}^n = 2L^0(N_t, N_t) \kappa_{c,LO}^{N_t}, \quad (61)$$

where $\kappa_{c,LO}$ is the leading-order critical point in two-flavor QCD. The critical lines calculated with $n_{\max} = 6-20$ are shown in Fig. 10 using $\kappa_{c,LO}$ obtained on the $24^3 \times 6$ (left) and $32^3 \times 6$ (right) lattices. The critical line converges well when $n_{\max} \gtrsim 10$.

5.4 Correlation among Wilson loops

Finally, we study the correlation among Wilson loops. Figure 11 shows the double distribution of $W(n)/W^0(n)$ and the plaquette \hat{P} measured at $\beta = 5.881$ and 5.900 on the $32^3 \times 6$ lattice. In the top left, top middle, \dots , and bottom right panels, the results for $n = 4, 6, 8, \dots$, and 20 are shown, respectively. The top left panel shows that the numerical result of $W(4)/W^0(4)$ is equal to the plaquette \hat{P} within the error of the noise method. We find that, though the $W(6)/W^0(6)$ data (the top middle panel) shows a strong linear correlation with \hat{P} , the correlation becomes gradually weak as n increases. Similar results are obtained in the calculation on the $32^3 \times 8$ lattice.

For small n , say $n \lesssim 10$, for which the linear correlation with \hat{P} is strong, we may approximate $W(n)$ as

$$W(n) \approx W^0(n) (d_n \hat{P} + f_n), \quad (62)$$

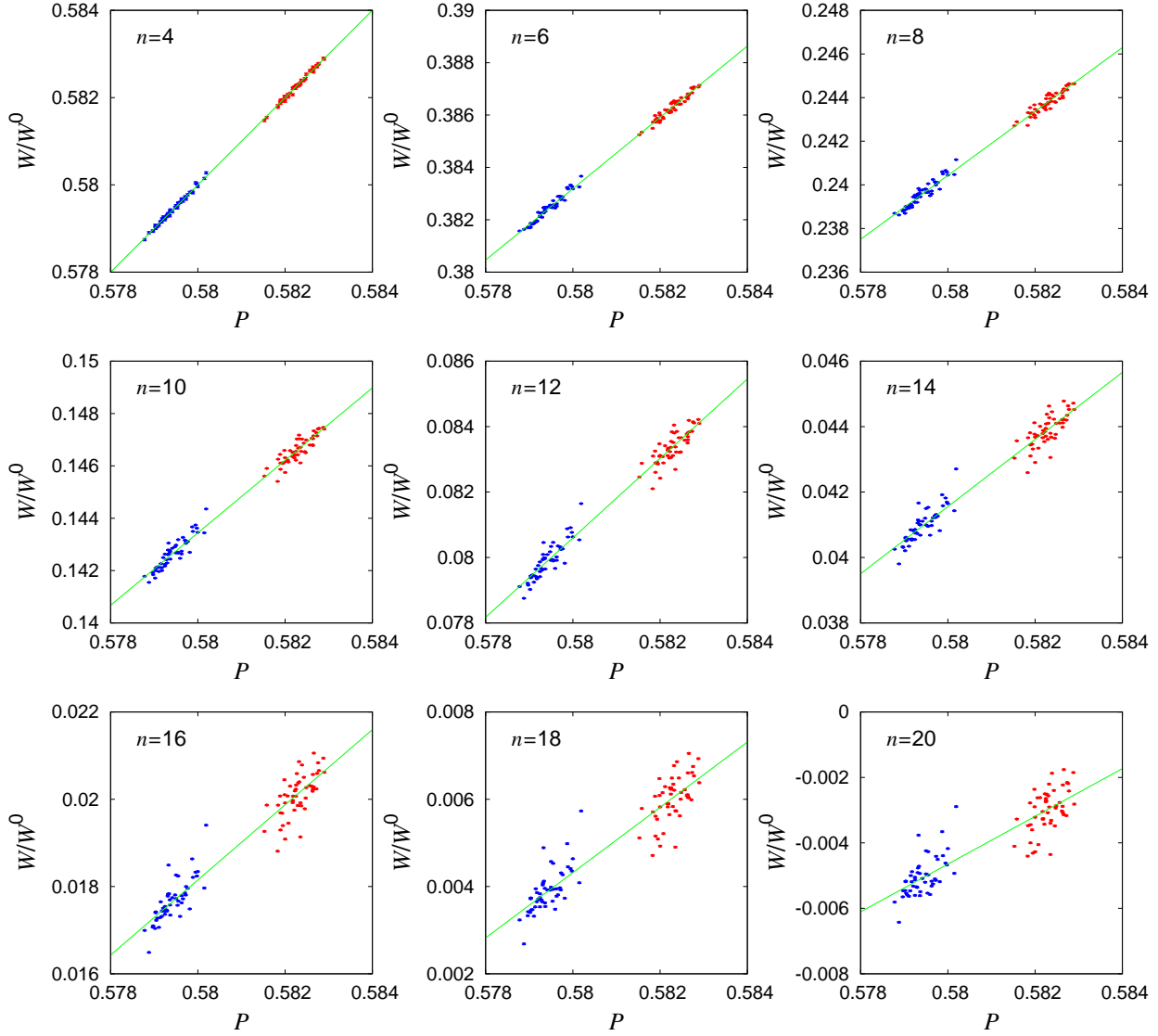


Fig. 11 Double distribution of the Wilson loop term $W(n)/W^0(n)$ and the plaquette \hat{P} in quenched QCD on a $32^3 \times 6$ lattice. The top left, top middle, \dots , and bottom right panels show the results of $n = 4, 6, \dots$, and 20 , respectively. Blue symbols are obtained at $\beta = 5.8810$, and red symbols at $\beta = 5.9000$, which are slightly below and above the phase transition point.

where $(d_4, f_4) = (1, 0)$ for the leading term $n = 4$. For $n \geq 6$, the coefficients d_n and f_n are obtained by fitting the data shown in Fig. 11 by Eq. (62). The results of the fits are shown by the green lines in Figs. 11 and listed in Table 5 together with the results of $N_t = 8$. As expected from the fact that $W^0(n)$ does not depend on N_t , the N_t dependence of the fit parameters d_n and f_n is quite small.

Table 5 Coefficients d_n and f_n of Eq. (62) obtained on $N_t = 6$ and 8 lattices. The numbers in the first parenthesis are the statistical errors by the jackknife method and those in the second parenthesis are the errors of the noise method.

n	$d_n(N_t = 6)$	$f_n(N_t = 6)$	$d_n(N_t = 8)$	$f_n(N_t = 8)$
4	1	0	1	0
6	1.3625(73)(12)	-0.4070(42)(7)	1.3366(66)(8)	-0.3922(39)(5)
8	1.4644(123)(11)	-0.6089(72)(6)	1.4256(96)(8)	-0.5869(57)(5)
10	1.3835(156)(10)	-0.6590(91)(6)	1.3433(117)(8)	-0.6367(70)(5)
12	1.2140(178)(9)	-0.6235(103)(5)	1.1752(130)(7)	-0.6025(78)(4)
14	1.0256(196)(9)	-0.5533(114)(5)	0.9825(141)(7)	-0.5303(85)(4)
16	0.8607(219)(9)	-0.4811(127)(5)	0.8052(153)(8)	-0.4512(92)(5)
18	0.7481(258)(10)	-0.4296(150)(6)	0.6698(173)(9)	-0.3870(103)(5)
20	0.7290(337)(12)	-0.4275(196)(7)	0.6071(219)(12)	-0.3606(131)(7)

Then, similarly to the effective theory discussed in Sec. 4.3, we may incorporate the effect of higher-order Wilson loop terms by a shift of β

$$\beta \longrightarrow \beta^* = \beta + \frac{1}{6} N_f \sum_{n=4}^{n_{\max}} W^0(n) d_n \kappa^n \quad (63)$$

in the gauge action. Here, the first correction term is for $n = 4$ and is just the $48N_f\kappa^4$ term in the right hand side of Eq. (47).

For n larger than about 10, because the correlation between $W(n)/W^0(n)$ and \hat{P} is not quite strong, the effect of $W(n)$ may not be well replaced by the shift of Eq. (63) only. However, as discussed in Sec. 4.1, the contribution of $n \gtrsim 10$ Wilson loops is small in the effective quark action up to $\kappa \lesssim 0.125$, and their remaining effect will be effectively absorbed by a small shift of improvement parameters of improved gauge action.

6 Critical point at non-zero densities

In Ref. [6], we studied the critical point of heavy quark QCD at non-zero density on an $N_t = 4$ lattice adopting the leading-order approximation of the hopping parameter expansion. As discussed in previous sections, the leading-order term is dominant around the critical point for $N_t = 4$ at zero density. Because the critical point moves toward smaller κ as the chemical potential increases, the results of Ref. [6] are reliable. To extend the study to larger values of N_t , however, we need to estimate the influence of higher-order terms.

With finite chemical potential μ , the Wilson quark kernel changes to

$$M_{xy}(\kappa) = \delta_{xy} - \kappa \left[\sum_{\mu=1}^3 \left\{ (1 - \gamma_\mu) U_{x,\mu} \delta_{y,x+\hat{\mu}} + (1 + \gamma_\mu) U_{y,\mu}^\dagger \delta_{y,x-\hat{\mu}} \right\} \right. \\ \left. + (1 - \gamma_4) U_{x,4} e^{+\mu a} \delta_{y,x+\hat{\mu}} + (1 + \gamma_4) U_{y,4}^\dagger e^{-\mu a} \delta_{y,x-\hat{\mu}} \right]. \quad (64)$$

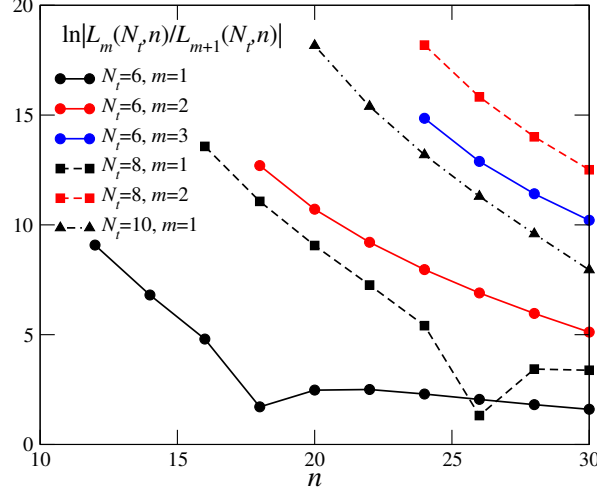


Fig. 12 Upper bound of μ/T that higher- m term is small, given in Eq. (69).

Because the link variables change as $U_{x,4} \rightarrow U_{x,4}e^{+\mu a}$ and $U_{x,4}^\dagger \rightarrow U_{x,4}^\dagger e^{-\mu a}$ in the quark kernel, L_m^+ and L_m^- change as $L_m^+ \rightarrow (e^{+\mu a})^{mN_t} L_m^+ = e^{+m\mu/T} L_m^+$ and $L_m^- \rightarrow (e^{-\mu a})^{mN_t} L_m^- = e^{-m\mu/T} L_m^-$, respectively, where, as introduced in Sec. 2, L_m^+ and $L_m^- = (L_m^+)^*$ are the parts of L_m going in the positive and negative directions, respectively. Therefore, the equation to determine the critical point is changed as follows,

$$\sum_{n=N_t}^{n_{\max}} \sum_{m=1}^{\infty} \left[L_m^+(N_t, n) e^{+m\mu/T} + L_m^-(N_t, n) e^{-m\mu/T} \right] \kappa_c^n = L^0(N_t, N_t) \kappa_{c, \text{LO}}^n \text{Re}\hat{\Omega}. \quad (65)$$

Corresponding to the effective theory discussed in Sec. 4.3 based on the strong correlation among the Polyakov-type loops, let us assume that

$$L_m^+(N_t, n) \approx \frac{1}{2} L_m^0(N_t, n) c_{n,m} \text{Re}\hat{\Omega}, \quad (66)$$

where $c_{n,m}$ is a constant to be determined by a Monte Carlo simulation. Then, Eq. (65) becomes

$$\frac{1}{2} \sum_{n=N_t}^{n_{\max}} \sum_{m=1}^{\infty} L_m^0(N_t, n) \left(c_{n,m} e^{+m\mu/T} + c_{n,m}^* e^{-m\mu/T} \right) \kappa_c^n = L^0(N_t, N_t) \kappa_{c, \text{LO}}^n. \quad (67)$$

The leading-order calculation of Ref. [6] for $N_t = 4$ corresponds to the case that the effect from $m \geq 2$ is negligible. To judge the magnitude of the effect from higher- m terms, we again consider the case of the worst convergence with $U_{x,\mu} = \mathbf{1}$. In this case, because $c_{n,m} = 1$, Eq. (67) reads

$$\sum_{n=N_t}^{n_{\max}} \sum_{m=1}^{\infty} L_m^0(N_t, n) \left(\cosh \frac{m\mu}{T} \right) \kappa_c^n = L^0(N_t, N_t) \kappa_{c, \text{LO}}^n. \quad (68)$$

Though $L_m^0(N_t, n)$ decreases as m increases, $\cosh(m\mu/T)$ may be large when μ/T is not small. Approximating $\cosh(m\mu/T) \approx e^{m\mu/T}$ for $m\mu/T > 1$, we find

$$\frac{\mu}{T} < \ln \left| \frac{L_m^0(N_t, n)}{L_{m+1}^0(N_t, n)} \right| \quad (69)$$

as a condition that the effect of higher- m term is small. In Fig. 12, we show the right hand side of Eq. (69) computed from Table 2. The circle, square and triangle symbols are the results for $N_t = 6, 8$ and 10 , respectively. The black, red and blue lines mean $m = 1, 2$ and 3 . When μ/T exceeds these values, effects of higher- m terms should be incorporated.

7 Summary and conclusions

We studied the convergence and the valid range of the hopping parameter expansion in the determination of the critical point (critical quark mass) of finite-temperature QCD with heavy quarks at which the first-order deconfinement transition in the heavy quark limit turns into crossover at intermediate quark masses. Adopting the standard plaquette gauge action and the standard Wilson quark action, we expand the effective quark action $\ln \det M$ by the hopping parameter κ around the heavy quark limit $\kappa = 0$, with $M(\kappa)$ the Wilson quark kernel. Non-vanishing contributions to the expansion terms are given by closed loops of the hopping term $B = -\partial M / \partial \kappa$. We classified the closed loops by the winding number m in the temporal direction, and decomposed each expansion term into Wilson loop term ($m = 0$) and Polyakov-type loop terms ($m \neq 0$). We developed a general method to calculate Wilson and Polyakov-type loop terms from the expansion terms with various twisted boundary conditions in the temporal direction.

To study the convergence of the hopping parameter expansion, we first studied the case of the worst convergence in which all the gauge link variables are unit matrices and thus the Wilson loops and the Polyakov-type loops get their maximum values. Our explicit calculation of the Wilson and Polyakov-type loop terms up to the 100th order of the hopping parameter expansion shows that the hopping parameter expansion is convergent up to around the chiral limit of free Wilson quarks, $\kappa = 0.125$, meaning that the convergence radius of the hopping parameter expansion is not small.

In practice, however, we need to truncate the expansion at some finite order and have to take into account the systematic error due to the truncation. We thus studied the issue of the truncation error of the hopping parameter expansion, focusing on the determination of the critical point κ_c in heavy quark QCD. In the case of worst convergence, we found that, the truncation error on $N_t = 4$ lattices is well under control up to around $\kappa \sim 0.1$, ensuring the previous next-to-leading order calculations of κ_c for $N_t = 4$ [5, 6]. We also found that the truncation error increases as N_t increases, such that, already for $N_t = 6$, significant effect from higher-order terms exist around κ_c determined by a next-to-leading order calculation.

To extend the valid range of the hopping parameter expansion, we thus revisit the effective theory of Refs. [5–7] which incorporates the next-to-leading effect into the leading-order calculation, and extend it to higher-orders of the hopping parameter expansion. We also discussed that the effect of Wilson loop terms can be represented by a shift of coupling parameters in the gauge action. The effective theory is based on the strong correlation between the leading-order Polyakov loop and next-to-leading bend Polyakov loops. By a Monte-Carlo simulation, we showed that the strong correlation holds also for higher-order Polyakov-type loops. We thus extended the effective theory to include higher-order terms of the hopping parameter expansion, and determined the coefficients needed in the effective theory. Using the effective theory, we discussed that the truncation error of the hopping parameter expansion is well under control for $\kappa \lesssim 0.125$ when the higher-order effect is incorporated into the effective theory up to sufficiently high orders. We evaluated the higher-order

correction of the critical point κ_c for $N_t = 6$. We also derived formulae for the critical point with general number of flavors at zero and finite densities.

In this paper, we have discussed the application of the hopping parameter expansion to the reweighting factor Eq. (46) for quenched QCD configurations. Besides the truncation error of the hopping parameter expansion, applicability range of the method is limited also by the overlapping problem of the reweighting method [5–7]. Here, we note that the effective theory we developed is applicable also to generate configurations effectively incorporating dynamical quark effect up to n_{\max} -th order of the hopping parameter expansion:

$$S_{\text{eff}} = -2N_c N_{\text{site}} \beta^* \hat{P} - N_s^3 \lambda \text{Re} \hat{\Omega} \quad \text{with} \quad \lambda = N_f N_t L^0(N_t, N_t) (\kappa^*)^{N_t}, \quad (70)$$

where β^* and κ^* are given by Eqs. (63) and (51), respectively. As performed in Ref. [8], Monte Carlo simulation with this action can be carried out efficiently. Because the Polyakov loop $\hat{\Omega}$ is the order parameter of the deconfinement transition of QCD in the heavy quark limit, incorporation of its effect into the configuration can lead to drastic improvements in the lattice study of the QCD phase transition. In Ref. [8], it was shown that the configuration generated by Eq. (70) with the leading-order β^* and κ^* removes the overlapping problem in the reweighting to incorporate the next-to-leading order effect. Effective inclusion of higher-order effect in the configuration will help achieving the high orders of the hopping-parameter expansion required in a study of κ_c for large values of N_t , thus extending the scope of the hopping parameter expansion.

Acknowledgments

The authors thank the members of the WHOT-QCD Collaboration for useful discussions. This work was in part supported by JSPS KAKENHI Grant Numbers JP21K03550, JP20H01903, JP19K03819, JP19H05146, and JP19H05598, the HPCI System Research project (Project ID: hp200089, hp210039), and Joint Usage/Research Center for Interdisciplinary Large-scale Information Infrastructures in Japan (JHPCN) (Project ID: jh200049).

References

- [1] I. R. McDonald and K. Singer, Discuss. Faraday Soc. **43**, 40 (1967); A. M. Ferrenberg and R. H. Swendsen, Phys. Rev. Lett. **61**, 2635 (1988); *ibid.* **63**, 1195 (1989).
- [2] C. R. Allton, S. Ejiri, S. J. Hands, O. Kaczmarek, F. Karsch, E. Laermann, C. Schmidt and L. Scorzato, Phys. Rev. D **66**, 074507 (2002).
- [3] S. Ejiri, Phys. Rev. D **69**, 094506 (2004).
- [4] R. Iwami, S. Ejiri, K. Kanaya, Y. Nakagawa, D. Yamamoto and T. Umeda, Phys. Rev. D **92**, no.9, 094507 (2015).
- [5] H. Saito, S. Ejiri, S. Aoki, T. Hatsuda, K. Kanaya, Y. Maezawa, H. Ohno, T. Umeda, Phys. Rev. D **84**, 054502 (2011) [erratum: Phys. Rev. D **85**, 079902 (2012)].
- [6] H. Saito, S. Ejiri, S. Aoki, K. Kanaya, Y. Nakagawa, H. Ohno, K. Okuno and T. Umeda, Phys. Rev. D **89**, no.3, 034507 (2014).
- [7] S. Ejiri, S. Itagaki, R. Iwami, K. Kanaya, M. Kitazawa, A. Kiyohara, M. Shirogane, T. Umeda, Phys. Rev. D **101**, no.5, 054505 (2020).
- [8] A. Kiyohara, M. Kitazawa, S. Ejiri and K. Kanaya, [arXiv:2108.00118 [hep-lat]].
- [9] S. Ejiri and N. Yamada, Phys. Rev. Lett. **110**, no.17, 172001 (2013).
- [10] S. Ejiri, R. Iwami and N. Yamada, Phys. Rev. D **93**, no.5, 054506 (2016).
- [11] F. Cuteri, O. Philipsen, A. Schön and A. Sciarra, Phys. Rev. D **103**, no.1, 014513 (2021).
- [12] R. Kara, S. Borsanyi, Z. Fodor, J. N. Guenther, P. Parotto, A. Pasztor and D. Sexty, [arXiv:2112.04192 [hep-lat]].
- [13] Y. Iwasaki, UTHEP-118 (1983) [arXiv:1111.7054 [hep-lat]]. Y. Iwasaki, Nucl. Phys. B **258**, 141 (1985).

- [14] K. Symanzik, in Mathematical problems in theoretical physics, eds. R. Schrader, R. Seiler, D. A. Uhlenbrock, Springer Lecture Notes in Physics, Vol. 153, 47 (1982); G. Curci, P. Menotti, and G. Paffuti, Phys. Lett. B 130, 205 (1983); M. Lüscher and P. Weisz, Commun. Math. Phys. 97, 59. [Erratum-ibid. 98, 433 (1985)]; M. Lüscher and P. Weisz, Phys. Lett. B 158, 250 (1985).
- [15] Y. Takaishi, Phys. Rev. D 54, 1050 (1996); P. de Forcrand, M. Garcia Perez, T. Hashimoto, S. Hioki, H. Matsufuru, O. Miyamura, A. Nakamura, I.O. Stamatescu, T. Takaishi and T. Umeda, Nucl. Phys. B 577, 263 (2000).
- [16] P. Hasenfratz and F. Niedermayer, Nucl. Phys., B 414, 785 (1994); T. DeGrand, A. Hasenfratz, P. Hasenfratz, F. Niedermayer, Nucl. Phys. B 454, 587 (1995); M. Blatter and F. Niedermayer, Nucl. Phys. B 482, 286 (1996).
- [17] M. Shirogane, S. Ejiri, R. Iwami, K. Kanaya and M. Kitazawa, Phys. Rev. D **94**, no.1, 014506 (2016).